Available online at www.sciencedirect.com
ScienceDirect
Journal of Sound and Vibration 298 (2006) 43–72
JOURNAL OF SOUND AND VIBRATION
www.elsevier.com/locate/jsvi

Theory and experiments for large-amplitude vibrations of circular cylindrical panels with geometric imperfections

M. Amabili*

Dipartimento di Ingegneria Industriale, Università di Parma, Parco Area delle Scienze 181/A, Parma 43100, Italy

Received 14 July 2005; received in revised form 19 April 2006; accepted 21 April 2006
Available online 17 August 2006

Abstract

Large-amplitude vibrations of circular cylindrical panels (open shells) subjected to harmonic excitation are numerically and experimentally investigated. The Donnell nonlinear strain–displacement relationships are used to describe the geometric nonlinearity; in-plane inertia is taken into account. Specific boundary conditions, with zero transverse displacement at the panel edges and free or elastically restrained in-plane displacements, not previously considered, have been introduced in order to model the experimental boundary conditions. The nonlinear equations of motion are obtained by the Lagrange equations with multi-mode approach, and are studied by using a code based on the pseudo-arclength continuation method. Two thin circular cylindrical panels of different dimensions and made of stainless steel have been experimentally tested in the laboratory for several excitation amplitudes in order to characterize the nonlinearity. The dimensions of the two panels have been chosen in order to have the fundamental mode with one and two circumferential half-waves, respectively. Numerical results are able to reproduce the experimental results with high accuracy for both panels. The effect of geometric imperfections on the trend of nonlinearity and on natural frequencies is shown; convergence of the solution with the number of generalized coordinates is numerically verified.

1. Introduction

Extensive literature review on the nonlinear vibration of circular cylindrical shells and panels is given by Amabili and Païdoussis [1]. Reissner [2], Grigolyuk [3] and Cummings [4] were pioneers in the study of large-amplitude vibrations of classical simply supported (in-plane free normal displacement and fixed tangential displacement at the edges), circular cylindrical shallow-shells using the Donnell nonlinear shallow-shell theory with a single-mode approximation. Leissa and Kadi [5] studied linear and nonlinear free vibrations of shallow doubly curved panels, classical simply supported at the four edges. The Donnell nonlinear shallow-shell theory was used in a slightly modified version to take into account the meridional curvature. A single mode expansion of the transverse displacement was used and the analysis was limited to the mode with one circumferential and one longitudinal half-wave, i.e. mode (1,1); actually results for higher modes are very scarce in the literature even today.

*Tel.: +39 0521 905896; fax: +39 0521 905705.
E-mail address: marco.amabili@unipr.it.
URL: http://me.unipr.it/mam/amabili/amabili.html.

0022-460X/$ - see front matter © 2006 Elsevier Ltd. All rights reserved.
doi:10.1016/j.jsv.2006.04.038

Other studies are due to Vol'mir et al. [6], Hui [7], Librescu and Chang [8], Chia [9], Fu and Chia [10], Raouf [11], Raouf and Palazotto [12], Yamaguchi and Nagai [13], and Popov et al. [14] and are discussed in [1]. Nagai et al. [15] extended their study on shallow shell reported in [13] to take into account a concentrated mass placed at the center of a panel. Experimental and numerical results are reported but the study is mainly focused on chaotic response, which is the main aim of their investigation. For this reason the trend of nonlinearity of the panel was not experimentally investigated.

Kobayashi and Leissa [16] studied free vibrations of mode (1,1) of doubly curved thick shallow panels; they used the nonlinear first-order shear deformation theory of shells in order to study thick shells. The rectangular boundaries of the panel were assumed to be classical simply supported at the four edges. A single mode expansion was used; in-plane and rotational inertia were neglected. Numerical results were obtained for circular cylindrical, spherical and paraboloidal panels. Except for hyperbolic paraboloid shells, a softening behaviour was found, becoming hardening for vibration amplitudes of the order of the shell thickness. However, increasing the radius of curvature, i.e. approaching a flat plate, the behaviour changed and became hardening. These results were proven to be accurate in the recent study of Amabili [17], where large-amplitude forced vibrations of mode (1,1) of circular cylindrical panels with rectangular base, classical simply supported at the four edges and subjected to radial harmonic excitation, are investigated. Two different nonlinear strain–displacement relationships, from the Donnell and the Novozhilov shell theories, are used to calculate the elastic strain energy. In-plane inertia and geometric imperfections are taken into account. The solution is obtained by the Lagrangian approach. Convergence of the solution is shown and differences between the Donnell and the Novozhilov nonlinear shell theories were fully negligible. Interaction of modes having integer ratio among their natural frequencies, giving rise to internal resonances, is also discussed.

Free vibrations of doubly curved, laminated, clamped shallow panels, including circular cylindrical panels, were studied by Abe et al. [18]. Both the first-order shear deformation theory and a classical shell theory analogous to the Donnell theory were used. The results obtained by neglecting in-plane and rotary inertia are very close to those obtained by retaining these effects. Only two modes were considered to interact in the nonlinear analysis for higher modes, while a single mode was used for the mode with one circumferential and one longitudinal half-wave. Results show only strong hardening type nonlinearity for mode (1,2).

In contrast with the amount of literature published on this topic, experimental results are very scarce and those reported by Amabili [19] seem to be the most suitable to reconstruct the trend of nonlinearity. However, the frame used in Ref. [19] to hold the panel gives boundary conditions on curved edges very difficult to be numerically simulated because the constraint is not bilateral; in fact, axially the panel cannot elongate due to pre-compression of the frame, but it can shrink axially at the edges.

As a consequence of this lack of experiments in the literature, a new series of experiments has been developed by using more sophisticated instrumentation; measurement of the actual surface geometry of the experimental panel has been carried out; based on the past experience, see [19], a new frame has been designed in order to hold the panel. The present paper synthesizes the experimental results, the theory developed and the numerical simulations. Specific boundary conditions, with zero transverse displacement at the panel edges and free or elastically restrained in-plane displacements, not previously considered in the literature, have been introduced in order to model the experimental boundary conditions. Results for this boundary condition are compared to nonlinear results for classical simply supported edges. Two thin circular cylindrical panels of different dimensions and made of stainless-steel have been experimentally tested in laboratory for several excitation amplitudes in order to characterize the nonlinearity. The dimensions of the two panels has been chosen in order to have the fundamental mode with one (1,1) and two (1,2) circumferential half-waves, respectively. Numerical results are able to reproduce the experimental results with high accuracy for both panels. The effect of geometric imperfections on the trend of nonlinearity and on natural frequencies is shown; convergence of the solution with the number of generalized coordinates is numerically verified.

2. Elastic strain energy of the panel

A circular cylindrical panel with the cylindrical coordinate system $(O;x,r,\theta)$, having the origin O at the center of one end of the panel, is considered, as shown in Fig. 1. The displacements of an arbitrary point of coordinates (x,θ) on the middle surface of the panel are denoted by u, v and w, in the axial, circumferential and

radial directions, respectively; w is taken positive outwards. Initial imperfections of the circular cylindrical panel associated with zero initial tension are denoted by radial displacement w_0, also positive outwards; only radial initial imperfections are considered.

The Donnell strain-displacement relationships for thin shells, based on the Love's first approximation assumptions, are used; in fact, in Ref. [17] it has been shown that they give the same results of the much more complex Novozhilov shell theory, saving computational time. The strain components ε_x, ε_θ and $\gamma_{x\theta}$ at an arbitrary point of the panel are related to the middle surface strains $\varepsilon_{x,0}$, $\varepsilon_{\theta,0}$ and $\gamma_{x\theta,0}$ and to the changes in the curvature and torsion of the middle surface k_x, k_θ and $k_{x\theta}$ by the following three relationships

$$\varepsilon_x = \varepsilon_{x,0} + zk_x, \quad \varepsilon_\theta = \varepsilon_{\theta,0} + zk_\theta, \quad \gamma_{x\theta} = \gamma_{x\theta,0} + zk_{x\theta}, \tag{1}$$

where z is the distance of the arbitrary point of the panel from the middle surface. The middle surface strain–displacement relationships and changes in the curvature and torsion for a circular cylindrical panel are [17]

$$\varepsilon_{x,0} = \frac{\partial u}{\partial x} + \frac{1}{2}\left(\frac{\partial w}{\partial x}\right)^2 + \frac{\partial w}{\partial x}\frac{\partial w_0}{\partial x}, \tag{2a}$$

$$\varepsilon_{\theta,0} = \frac{\partial v}{R\partial\theta} + \frac{w}{R} + \frac{1}{2}\left(\frac{\partial w}{R\partial\theta}\right)^2 + \frac{\partial w}{R\partial\theta}\frac{\partial w_0}{R\partial\theta}, \tag{2b}$$

$$\gamma_{x\theta,0} = \frac{\partial u}{R\partial\theta} + \frac{\partial v}{\partial x} + \frac{\partial w}{\partial x}\frac{\partial w}{R\partial\theta} + \frac{\partial w}{\partial x}\frac{\partial w_0}{R\partial\theta} + \frac{\partial w_0}{\partial x}\frac{\partial w}{R\partial\theta}, \tag{2c}$$

$$k_x = -\frac{\partial^2 w}{\partial x^2}, \tag{2d}$$

$$k_\theta = -\frac{\partial^2 w}{R^2\partial\theta^2}, \tag{2e}$$

$$k_{x\theta} = -2\frac{\partial^2 w}{R\partial x\partial\theta}. \tag{2f}$$

The elastic strain energy U_S of a circular cylindrical panel, neglecting σ_z as stated by Love's first approximation assumptions, is given by

$$U_S = \frac{1}{2}\int_0^\alpha \int_0^a \int_{-h/2}^{h/2} \left(\sigma_x\varepsilon_x + \sigma_\theta\varepsilon_\theta + \tau_{x\theta}\gamma_{x\theta}\,\mathrm{d}z\,\mathrm{d}x\,R(1+z/R)\,\mathrm{d}\theta\right), \tag{3}$$

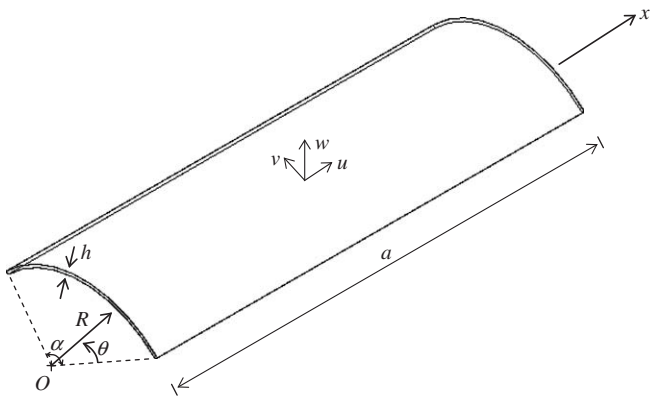

Fig. 1. Geometry of the panel, coordinate system and symbols.

where h is the panel thickness, R is the panel middle radius, a is the panel length, α is the angular dimension of the panel and the stresses σ_x, σ_θ and $\tau_{x\theta}$ are related to the strains for homogeneous and isotropic material ($\sigma_z = 0$, case of plane stress) by

$$\sigma_x = \frac{E}{1-\nu^2}(\varepsilon_x + \nu\,\varepsilon_\theta), \quad \sigma_\theta = \frac{E}{1-\nu^2}(\varepsilon_\theta + \nu\,\varepsilon_x), \quad \tau_{x\theta} = \frac{E}{2(1+\nu)}\gamma_{x\theta}, \tag{4}$$

where E is the Young's modulus and ν is the Poisson's ratio. By using Eqs. (1)–(4), the following expression is obtained:

$$U_S = \frac{1}{2}\frac{Eh}{1-\nu^2}\int_0^\alpha\int_0^a\left(\varepsilon_{x,0}^2 + \varepsilon_{\theta,0}^2 + 2\nu\,\varepsilon_{x,0}\,\varepsilon_{\theta,0} + \frac{1-\nu}{2}\gamma_{x\theta,0}^2\right)\mathrm{d}x\,R\,\mathrm{d}\theta$$
$$+\frac{1}{2}\frac{Eh^3}{12(1-\nu^2)}\int_0^\alpha\int_0^a\left(k_x^2 + k_\theta^2 + 2\nu\,k_x\,k_\theta + \frac{1-\nu}{2}k_{x\theta}^2\right)\mathrm{d}x\,R\,\mathrm{d}\theta + O(h^4), \tag{5}$$

where $O(h^4)$ is a higher-order term in h: the first term is the membrane (also referred to as stretching) energy and the second one is the bending energy.

3. Boundary conditions, kinetic energy, external loads and mode expansion

The kinetic energy T_S of a circular cylindrical panel, by neglecting rotary inertia, is given by

$$T_S = \frac{1}{2}\rho_S h\int_0^\alpha\int_0^a(\dot{u}^2 + \dot{v}^2 + \dot{w}^2)\,\mathrm{d}x\,R\,\mathrm{d}\theta, \tag{6}$$

where ρ_s is the mass density of the panel. In Eq. (10) the overdot denotes a time derivative.

The virtual work W done by the external forces is written as

$$W = \int_0^\alpha\int_0^a\left(q_x u + q_\theta v + q_r w\right)\mathrm{d}x\,R\,\mathrm{d}\theta, \tag{7}$$

where q_x, q_θ and q_r are the distributed forces per unit area acting in axial, circumferential and radial directions, respectively. Only a single harmonic radial force is considered; therefore $q_x = q_\theta = 0$. The external radial distributed load q_r applied to the panel, due to the radial concentrated force $\tilde{f}$, is given by

$$q_r = \tilde{f}\,\delta(R\theta - R\tilde{\theta})\delta(x - \tilde{x})\,\cos(\omega t), \tag{8}$$

where ω is the excitation frequency, t is the time, δ is the Dirac delta function, $\tilde{f}$ gives the radial force amplitude positive in w direction, $\tilde{x}$ and $\tilde{\theta}$ give the axial and angular positions of the point of application of the force, respectively. Eq. (7) can be rewritten in the following form:

$$W = \tilde{f}\,\cos(\omega t)w|_{x=\tilde{x},\ \theta=\tilde{\theta}}. \tag{9}$$

The following boundary conditions are introduced in the present study:

$$N_x = w = w_0 = M_x = \partial^2 w_0/\partial x^2 = 0, \quad N_{x,y} = -kv, \quad \text{at } x = 0, a, \tag{10a–f}$$

$$N_y = w = w_0 = M_y = \partial^2 w_0/\partial\, y^2 = 0, N_{x,y} = -ku, \quad \text{at } y = 0, b, \tag{11a–f}$$

where $y = R\theta$, $b = R\alpha$, k is the distributed spring stiffness ($\mathrm{N/m^2}$) where springs are tangential to the panel edges and are distributed along the four boundaries, M_x and M_y are the bending moments per unit length on the edges orthogonal to x and y, respectively, N_x and N_y are the in-plane normal forces per unit length and $N_{x,y}$ is the in-plane shear force per unit length. Eqs. (10) and (11) give fully free in-plane boundary conditions for $k = 0$, and classical simply supported conditions in the limit case $k \to \infty$; w is zero at the four panel edges for any value of k; it can be observed that k can be a function of x and y, therefore giving non-uniform stiffness at the panel edges.

In order to reduce the system to finite dimensions, the middle surface displacements u, v and w are expanded by using the following approximate functions, which satisfy identically the geometric boundary conditions (10b, 11b):

$$w(x,y,t)=\sum_{m=1}^{M_1}\sum_{n=1}^{N_1} w_{m,n}(t)\,\sin(m\pi x/a)\,\sin(n\pi y/b), \tag{12}$$

$$u(x,y,t)=\sum_{m=1}^{M_2}\sum_{n=0}^{N_2} u_{m,n}(t)\,\cos(m\pi x/a)\,\cos(n\pi y/b), \tag{13}$$

$$v(x,y,t)=\sum_{m=0}^{M_3}\sum_{n=1}^{N_3} v_{m,n}(t)\,\cos(m\pi x/a)\,\cos(n\pi y/b), \tag{14}$$

where m and n are the numbers of half-waves in x and y directions, respectively, and t is the time; $u_{m,n}(t)$, $v_{m,n}(t)$ and $w_{m,n}(t)$ are the generalized coordinates that are unknown functions of t. M and N indicate the terms necessary in the expansion of the displacements.

Only transverse (radial) initial geometric imperfections of the panel are assumed; they are associated with zero initial stress. The imperfection w_0 is expanded in the same form of w, i.e. in a double Fourier sine series satisfying the boundary conditions ((10c,e) and (11c,e)) at the panel edges

$$w_0(x,y)=\sum_{m=1}^{\tilde{M}}\sum_{n=1}^{\tilde{N}} A_{m,n}\,\sin(m\pi x/a)\,\sin(n\pi y/b), \tag{15}$$

where $A_{m,n}$ are the modal amplitudes of imperfections; $\tilde{N}$ and $\tilde{M}$ are integers indicating the number of terms in the expansion.

4. Additional terms to satisfy the boundary conditions

The geometric boundary conditions, Eqs. (10b,c,e) and (11b,c,e), are exactly satisfied by the expansions of u, v, w and w_0. On the other hand, Eqs. (10d, 11d) can be rewritten in the following form [20]

$$M_x=\frac{Eh^3}{12(1-\nu^2)}(k_x+\nu k_\theta)=0 \quad \text{at } x=0,a, \tag{16}$$

$$M_y=\frac{Eh^3}{12(1-\nu^2)}(k_\theta+\nu k_x)=0 \quad \text{at } y=0,b. \tag{17}$$

Eqs. (16) and (17) are identically satisfied for the expressions of k_x and k_θ given in Eqs. (2d,e). Moreover, the following constraints, Eqs. (10a, 11a), must be satisfied [20]:

$$N_x=\frac{Eh}{1-\nu^2}\left(\varepsilon_{x,0}+\nu\varepsilon_{\theta,0}\right)=0 \quad \text{at } x=0,a, \tag{18}$$

$$N_y=\frac{Eh}{1-\nu^2}\left(\varepsilon_{\theta,0}+\nu\varepsilon_{x,0}\right)=0 \quad \text{at } y=0,b. \tag{19}$$

Eqs. (18) and (19) are not identically satisfied. Eliminating zero terms at the panel edges, Eqs. (18) and (19) can be rewritten as

$$\frac{\partial\hat{u}}{\partial x}+\frac{1}{2}\left(\frac{\partial w}{\partial x}\right)^2+\frac{\partial w}{\partial x}\frac{\partial w_0}{\partial x}+\nu\frac{\partial(v+\hat{v})}{\partial y}=0 \quad \text{at } x=0,a, \tag{20}$$

$$\frac{\partial\hat{v}}{\partial y}+\frac{1}{2}\left(\frac{\partial w}{\partial y}\right)^2+\frac{\partial w}{\partial y}\frac{\partial w_0}{\partial y}+\nu\frac{\partial(u+\hat{u})}{\partial x}=0 \quad \text{at } y=0,b, \tag{21}$$

where $\hat{u}$ and $\hat{v}$ are terms added to the expansion of u and v, given in Eqs. (13) and (14), in order to satisfy exactly the boundary conditions $N_x = 0$ and $N_y = 0$. The term v in Eq. (20) is eliminated because it gives a linear relationship between u and v, which is satisfied by using the minimization of energy in the process of building the Lagrange equations of motion; in fact, this is equivalent to the Rayleigh–Ritz method and therefore it requires to satisfy only geometrical boundary conditions. Similarly u is eliminated in Eq. (21). Therefore $\hat{u}$ and $\hat{v}$ are reduced to second-order terms in the panel displacement (assuming geometric imperfections of the same order of $w_{m,n}$); non-trivial calculations, reported in [17], give

$$\hat{u}(t) = -\sum_{n=1}^{N_1}\sum_{m=1}^{M_1}(m\,\pi/a)\left\{\frac{1}{2}w_{m,n}(t)\sin(n\pi y/b)\sum_{k=1}^{N_1}\sum_{s=1}^{M_1}\frac{s}{m+s}w_{s,k}(t)\,\sin(k\pi y/b)\,\sin\left[(m+s)\pi x/a\right]\right.$$
$$\left.+\,w_{m,n}(t)\,\sin(n\pi y/b)\sum_{j=1}^{\tilde{N}}\sum_{i=1}^{\tilde{M}}\frac{i}{m+i}A_{i,j}\,\sin(j\pi y/b)\,\sin\left[(m+i)\pi x/a\right]\right\}, \tag{22a}$$

$$\hat{v}(t) = -\sum_{n=1}^{N_1}\sum_{m=1}^{M_1}(n\,\pi/b)\left\{\frac{1}{2}w_{m,n}(t)\,\sin(m\pi x/a)\sum_{k=1}^{N_1}\sum_{s=1}^{M_1}\frac{k}{n+k}w_{s,k}(t)\,\sin(s\pi x/a)\,\sin\left[(n+k)\pi y/b\right]\right.$$
$$\left.+\,w_{m,n}(t)\,\sin(m\pi x/a)\sum_{j=1}^{\tilde{N}}\sum_{i=1}^{\tilde{M}}\frac{j}{n+j}A_{i,j}\,\sin(i\pi x/a)\,\sin\left[(n+j)\pi y/b\right]\right\}. \tag{22b}$$

Actually, Eqs. (20) and (21) can be satisfied by energy minimization by avoiding to introduce Eqs. (22). But the choice of the expansions of u and v become very tricky, i.e. all the terms involved in Eqs. (22) must be inserted in the expansion as additional degrees of freedom, in order to predict the system behaviour with accuracy. This has been verified numerically.

In the following part of the present paper, the axial displacement u will be given by $u + \hat{u}$, where u is given by Eq. (13) and $\hat{u}$ by Eq. (22a); similarly for v that will be given by $v + \hat{v}$.

Finally boundary conditions (10f, 11f) must be also satisfied. They give [20]

$$N_{x,y} = \frac{Eh}{2(1+\nu)}\gamma_{x,y} = -kv \quad \text{at } x = 0, a, \tag{23a}$$

$$N_{y,x} = \frac{Eh}{2(1+\nu)}\gamma_{y,x} = -ku \quad \text{at } y = 0, b. \tag{23b}$$

Eliminating zero terms at the panel edges, Eqs. (23) can be rewritten as

$$\frac{Eh}{2(1+\nu)}\left[\frac{\partial u}{\partial y}+\frac{\partial v}{\partial x}\right]_{x=0,a} = -kv \quad \text{at } x = 0, a, \tag{24a}$$

$$\frac{Eh}{2(1+\nu)}\left[\frac{\partial u}{\partial y}+\frac{\partial v}{\partial x}\right]_{y=0,b} = -ku \quad \text{at } y = 0, b. \tag{24b}$$

In case of zero stiffness of the distributed springs, $k = 0$, Eqs. (24) give a linear condition, which is satisfied by using minimization of energy in the Lagrange equations of motion. Therefore no additional terms in the expansion are introduced. In case of k different from zero, an additional potential energy stored by the elastic springs at the shell edges must be added. This potential energy U_K is given by

$$U_K = \frac{1}{2}\int_0^b k\left\{\left[(v)_{x=0}\right]^2 + \left[(v)_{x=a}\right]^2\right\}\mathrm{d}\,y + \frac{1}{2}\int_0^a k\left\{\left[(u)_{y=0}\right]^2 + \left[(u)_{y=a}\right]^2\right\}\mathrm{d}x. \tag{25}$$

In Eq. (25) a non-uniform stiffness k (simulating a non-uniform constraint) can be assumed. In order to simulate classical simply supported edges, corresponding to $v = 0$ at $x = 0, a$, and $u = 0$ at $y = 0, b$ a very high value of the stiffness k must be assumed.

5. Lagrange equations of motion

The nonconservative damping forces are assumed to be of viscous type and are taken into account by using the Rayleigh's dissipation function

$$F = \frac{1}{2}c\int_0^a\int_0^b \left(\dot{u}^2+\dot{v}^2+\dot{w}^2\right)\mathrm{d}x\,\mathrm{d}y, \tag{26}$$

where c has a different value for each term of the mode expansion. Simple calculations give

$$F = \frac{1}{2}(ab/4)\left[\sum_{n=1}^{N_1}\sum_{m=1}^{M_1} c_{m,n}\dot{w}_{m,n}^2+\sum_{n=1}^{N_2}\sum_{m=1}^{M_2} c_{m,n}\dot{u}_{m,n}^2+\sum_{n=1}^{N_3}\sum_{m=1}^{M_3} c_{m,n}\dot{v}_{m,n}^2\right]. \tag{27}$$

The damping coefficient $c_{m,n}$ is related to damping ratio, by $\varsigma_{m,n} = c_{m,n}/(2\,\mu_{m,n}\,\omega_{m,n})$, where $\omega_{m,n}$ is the natural circular frequency of mode (m, n) and $\mu_{m,n}$ is the modal mass of this generalized coordinate, given by $\mu_{m,n} = \rho_S\, h\,(ab/4)$.

The following notation is introduced for brevity

$$\mathbf{q} = \left\{u_{m,n}, v_{m,n}, w_{m,n}\right\}^{\mathrm{T}}, \quad m = 1,\ldots M_{1\text{ or }2\text{ or }3} \text{ and } n = 1,\ldots N_{1\text{ or }2\text{ or }3}. \tag{28}$$

The generic element of the time-dependent vector $\mathbf{q}$ is referred to as q_j, which is the generalized coordinate; the dimension of $\mathbf{q}$ is dofs, which is the number of degrees of freedom used in the mode expansion.

The generalized forces Q_j are obtained by differentiation of the Rayleigh's dissipation function and of the virtual work done by external concentrated harmonic force (in the following equation supposed to act at the center of the panel)

$$\begin{aligned} Q_j = & -\frac{\partial F}{\partial \dot{q}_j}+\frac{\partial W}{\partial q_j} = -(ab/4)c_j\dot{q}_j \\ & + \begin{cases} 0 & \text{if } q_j = u_{m,n},\ v_{m,n};\ \text{or}\ w_{m,n} \text{ with } m \text{ or } n \text{ even}, \\ \tilde{f}\cos(\omega t) & \text{if } q_j = w_{m,n} \text{ with both } m \text{ and } n \text{ odd}. \end{cases} \end{aligned} \tag{29}$$

The Lagrange equations of motion are

$$\frac{\mathrm{d}}{\mathrm{d}t}\left(\frac{\partial T_S}{\partial \dot{q}_j}\right)-\frac{\partial T_S}{\partial q_j}+\frac{\partial (U_S+U_K)}{\partial q_j} = Q_j, \quad j = 1,\ldots \text{dofs}, \tag{30}$$

where $\partial T_S \big/ \partial q_j = 0$. These second-order equations have very long expressions containing quadratic and cubic nonlinear terms.

If geometric imperfections have the same order of amplitude of $w_{m,n}$, $\hat{u}$ and $\hat{v}$ have amplitude of order $w_{m,n}^2$; therefore their contribution to the system inertia is neglected. In this case,

$$\frac{\mathrm{d}}{\mathrm{d}t}\left(\frac{\partial T_S}{\partial \dot{q}_j}\right) = \rho_S h(ab/4)\ddot{q}_j, \tag{31}$$

which shows that no inertial coupling among the Lagrange equations exists for the panel. In the present study in-plane inertia is taken into account; Amabili [21] investigated the effect of in-plane inertia on large-amplitude vibrations of a complete circular cylindrical shell, showing that in-plane inertia should be included to have an accurate model in that case. If panels are shallow, probably the effect of in-plane inertia is less important than for complete circular shells.

The very complicated term giving quadratic and cubic nonlinearities can be written in the form

$$\frac{\partial (U_S+U_K)}{\partial q_j} = \sum_{k=1}^{\text{dofs}} q_k f_{k,j}+\sum_{i,k=1}^{\text{dofs}} q_i q_k f_{i,k,j}+\sum_{i,k,l=1}^{\text{dofs}} q_i q_k q_l f_{i,k,l,j}, \tag{32}$$

where coefficients f have long expressions that include also geometric imperfections.

The equations of motion have been obtained by using the *Mathematica* computer software [22] in order to perform analytical surface integrals of trigonometric functions (e.g. integrals in Eq. (5)). The generic jth Lagrange equation is divided by the mass of the jth generalized coordinate (associated with $\ddot{q}_j$) and then is transformed in two first-order equations. A non-dimensionalization of variables is also performed for computational convenience: the frequencies are divided by the natural circular frequency $\omega_{m,n}$ of the mode (m, n) investigated, and the vibration amplitudes are divided by the panel thickness h. The resulting $2 \times$ dofs equations are studied by using (i) the software AUTO 97 [23] for continuation and bifurcation analysis of nonlinear ordinary differential equations and (ii) direct integration of the equations of motion by using the DIVPAG routine of the Fortran library IMSL. The software AUTO 97 allows continuation of the solution, bifurcation analysis and branch switching by using pseudo-arclength continuation and collocation methods; in the present study the program has been modified in order to handle more variables and it has been recompiled for PC. In particular, the panel response under harmonic excitation has been studied by using an analysis in two steps: (i) first the excitation frequency has been fixed far enough from resonance and the magnitude of the excitation has been used as bifurcation parameter; the solution has been started at zero force where the solution is the trivial undisturbed configuration of the panel and has been continued up to reach the desired

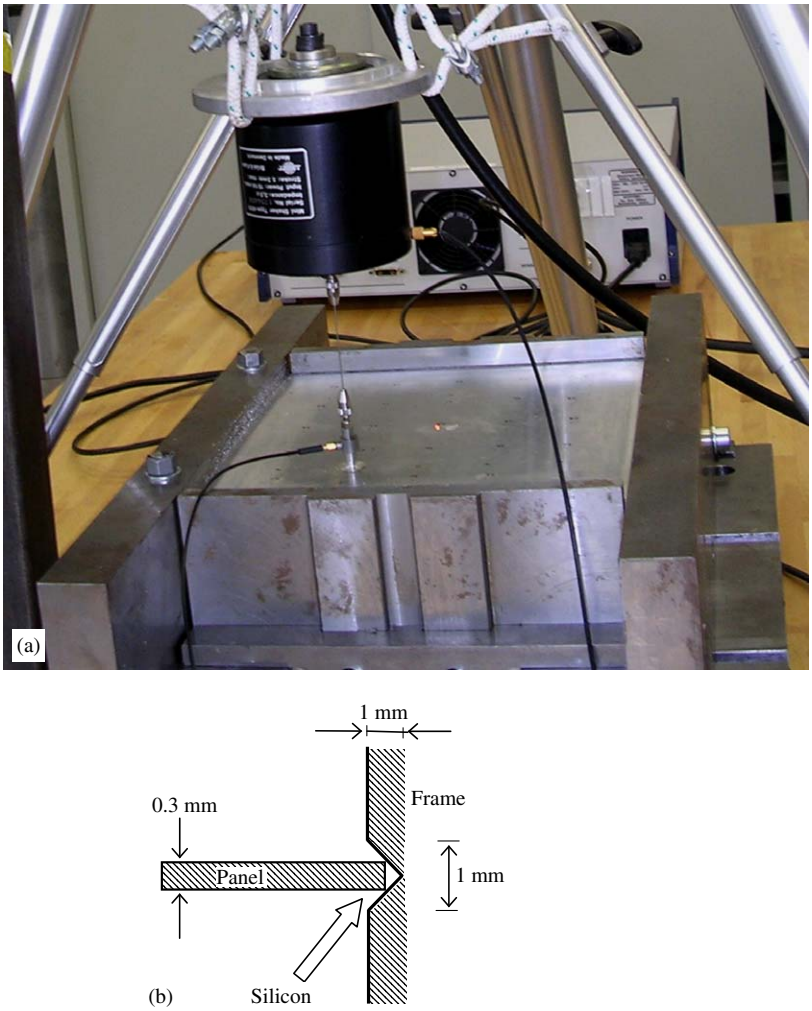

Fig. 2. (a) Photograph of the experimental panel B, connected to the shaker by the stinger and the load cell and (b) drawing of the panel inserted into the V-groove in the supporting frame.

force amplitude; (ii) when the desired amplitude of excitation has been reached, the solution has been continued by using the excitation frequency as bifurcation parameter.

The natural frequencies are obtained eliminating all the nonlinear terms from the equations of motion; then the equations are re-written in matrix form and the classical eigenvalue problem is solved by using *Mathematica*.

6. Laboratory experiments

Tests have been conducted on two stainless steel panels, panel A and panel B, with the following dimensions and material properties; panel A: $a = 0.\ 199\,\text{m}$, $R = 2\,\text{m}$, $\alpha = 0.066\cdot$, $h = 0.0003\,\text{m}$, $E = 195 \times 10^9\,\text{Pa}$, $\rho = 7800\,\text{kg/m}^3$ and $v = 0.3$; panel B: $a = 0.2\,\text{m}$, $R = 2\,\text{m}$, $\alpha = 0.1\cdot$, $h = 0.0003\,\text{m}$, $E = 195 \times 10^9\,Pa$, $\rho = 7800\,\text{kg/m}^3$ and $v = 0.3$. Therefore the two panels are almost identical, excluding the angular dimension α. These two different values have been chosen in order to have for panel A fundamental mode ($m = 1$, $n = 1$), and for panel B fundamental mode (1,2). Each panel was inserted into a heavy rectangular steel frame made of several thick parts, see Figs. 2(a) and (b), having V-grooves designed to hold the panel and to avoid transverse (radial) displacements at the edges; silicon was placed into the grooves to fill any gap between the panel and the grooves. Practically all the in-plane displacements normal to the edges were allowed because the constraint given by silicon on these displacements was very small; in-plane displacements parallel to the edges were

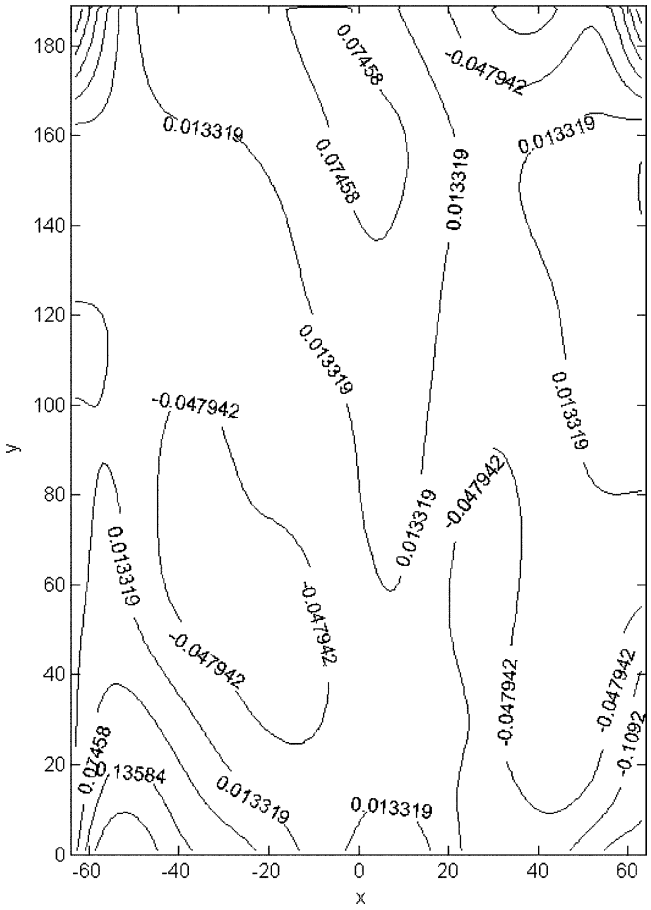

Fig. 3. Contour plot indicating measured geometric imperfections as deviation from the ideal panel A surface. Deviations are in millimeters.

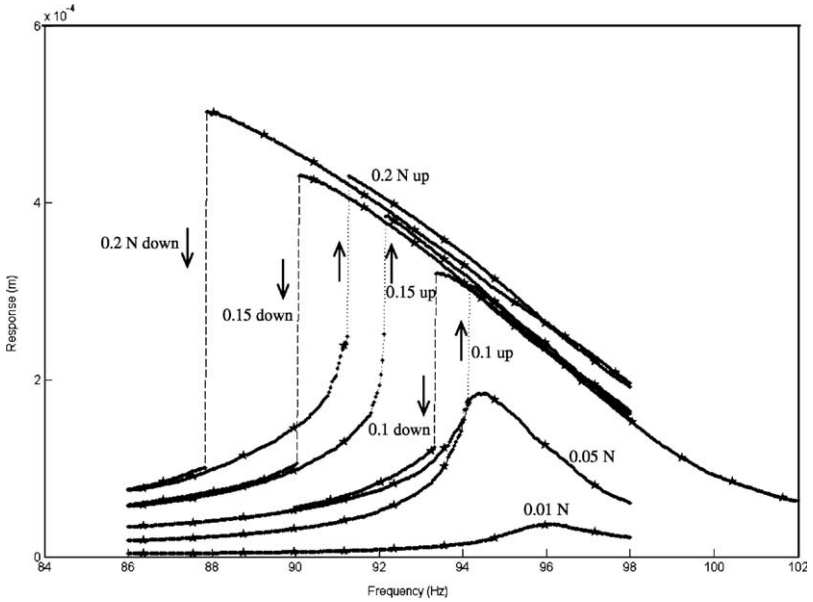

Fig. 4. Experimental oscillatory displacement (first harmonic) versus excitation frequency for different excitation levels measured at the center of the panel A; fundamental mode (1,1). ●, experimental point, - -, connecting line (down), …, connecting line (up), →, direction of movement along the line.

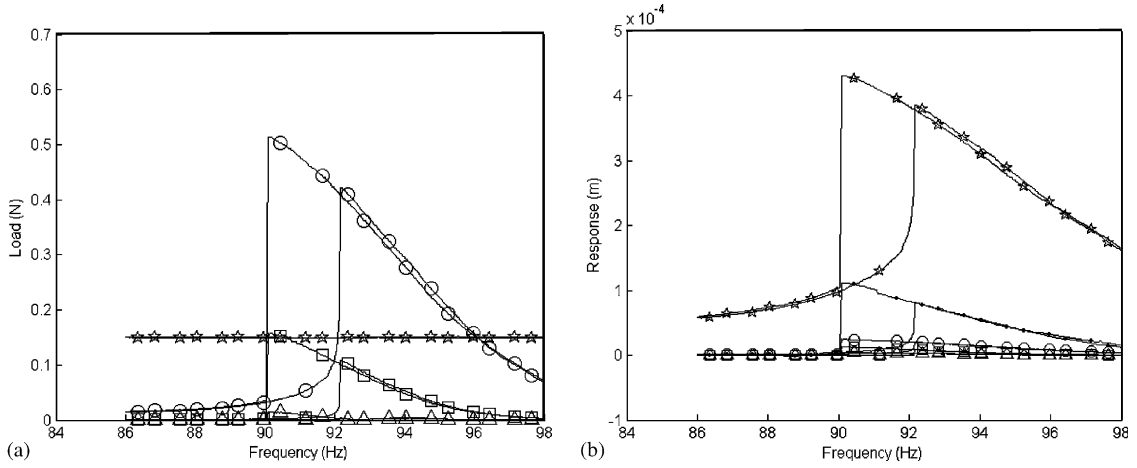

Fig. 5. Harmonic components of the excitation force and of the experimentally measured response of panel A; mode (1,1). ● = mean value; ☆ = first harmonic; ○ = second harmonic; □ = third harmonic; △ = fourth harmonic. (a) Excitation force 0.15 N and (b) measured response for excitation 0.15 N.

elastically constrained by the silicon. Therefore the experimental boundary conditions are close to those given by Eqs. (10) and (11), with k assuming a relatively small value.

The panels have been subjected to (i) burst-random excitation to identify the natural frequencies and perform a modal analysis by measuring the panel response on a grid of points, (ii) harmonic excitation, increasing or decreasing by very small steps the excitation frequency in the spectral neighbourhood of the lowest natural frequencies, to characterize nonlinear responses in presence of large-amplitude vibrations (step-sine excitation). The excitation has been provided by an electrodynamical exciter (shaker), model *B&K* 4810. A piezoelectric miniature force transducer *B&K* 8203 of the weight of 3.2 grams, glued to the panel and

connected to the shaker with a stinger, measured the force transmitted. The panel response has been measured by using a very accurate laser Doppler vibrometer Polytec (sensor head OFV-505 and controller OFV-5000) in order to have non-contact measurement without introduction of inertia. The time responses have been

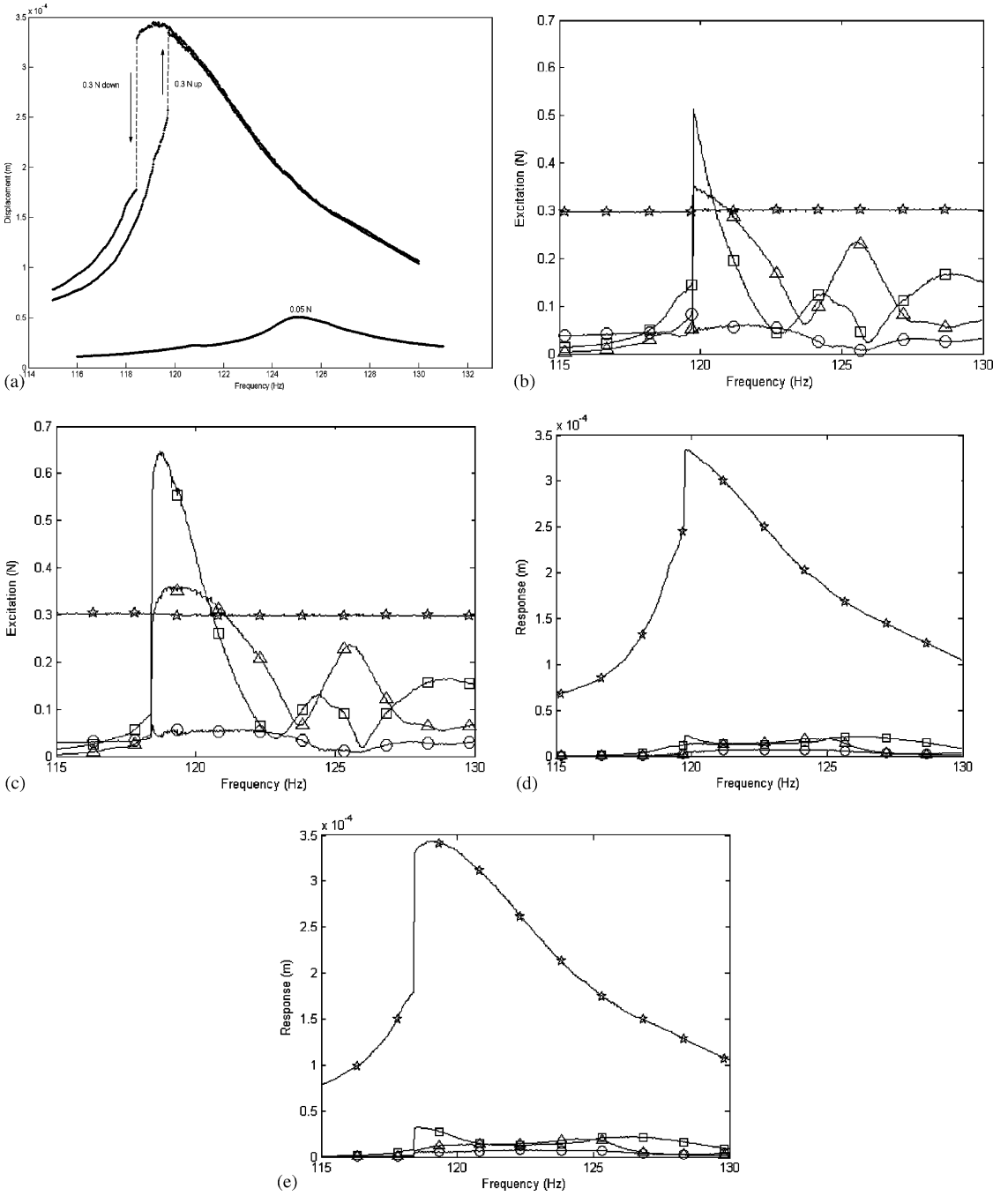

Fig. 6. Experimental results for panel B; fundamental mode (1,2). (a) Experimental oscillatory displacement (first harmonic) versus excitation frequency for two excitation levels measured at $x = a/2$, $y = 3/4b$. ○, experimental point; - -, connecting line; →, direction of movement along the line. (b) harmonic components of the excitation force 0.3 N up; (c) harmonic components of the excitation force 0.3 N down; (d) harmonic components of the response for excitation 0.3 N up; (e) harmonic components of the response for excitation 0.3 N down. ☆ = first harmonic; ○ = second harmonic; □ = third harmonic; △ = fourth harmonic.

measured by using the Difa Scadas II front-end, connected to a HP c3000 workstation, and the software CADA-X 3.5b of LMS for signal processing, data analysis, experimental modal analysis and excitation control. The same front-end has been used to generate the excitation signal. The CADA-X closed-loop control has been used to keep constant the value of the excitation force for any excitation frequency, during the measurement of the nonlinear response.

Geometric imperfections of the panel A have been detected by using a 3-D laser scanning system VI-910 Minolta to measure the actual panel surface. The contour plot indicating the deviation from the ideal panel surface is reported in Fig. 3. Geometric imperfections are always present in actual panels. Actually in the tested panels these imperfections are associated to initial stresses, which have been minimized with accurate positioning in the frame. These initial stresses are not measured and are not taken into account in the modelling. No measurement of imperfection has been made on panel B.

6.1. Nonlinear results for panel A

Fig. 4 shows the measured oscillation (displacement, directly measured by using the Polytec laser Doppler vibrometer with displacement decoder DD-200 in the OFV-5000 controller; measurement position at the center of the panel) around the fundamental frequency, i.e. mode (1,1), versus the excitation frequency for three different force levels: 0.01, 0.05, 0.1, 0.15 and 0.2 N. The excitation point was at $\tilde{x} = a/4$ and $\tilde{y} = b/3$. The level of 0.01 N gives a good evaluation of the natural (linear) frequency, identified at 96.2 Hz. The closed-loop control used in the experiments keeps constant the amplitude of the harmonic excitation force, after filtering the signal from the load cell in order to use only the harmonic component with the given excitation frequency. The measured oscillation reported in Fig. 4 has been filtered in order to eliminate any frequency except the excitation frequency (first harmonic of the response). Experiments have been performed increasing and decreasing the excitation frequency (up and down); the frequency step used in this case is 0.025 Hz,

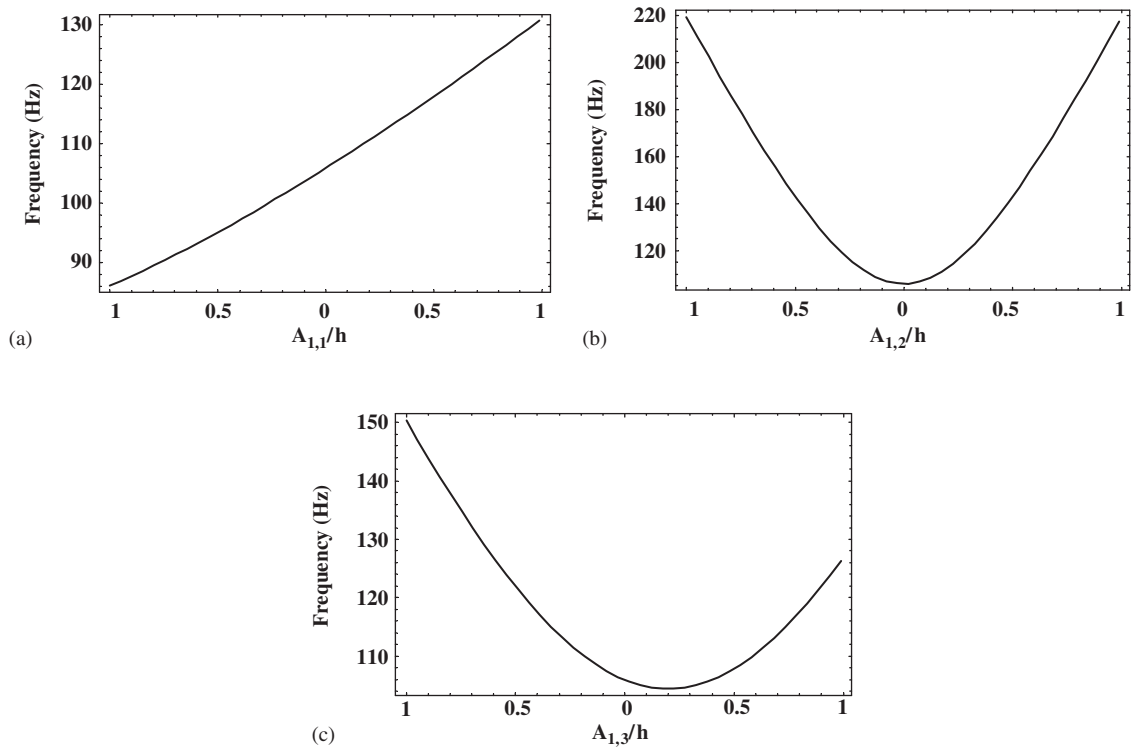

Fig. 7. Natural frequency of the fundamental mode (1,1) of panel A versus geometric imperfections; 13 dofs model, $k = 0$. (a) Effect of $A_{1,1}$; (b) effect of $A_{1,2}$; (c) effect of $A_{1,3}$.

16 periods have been measured with 128 points per period and 200 periods have been waited before data acquisition every time that the frequency is changed. The hysteresis between the two curves (up = increasing frequency; down = decreasing frequency) is clearly visible for the three larger excitation levels (0.1, 0.15 and 0.2 N). Sudden increments (jumps) of the vibration amplitude are observed when increasing and decreasing the excitation frequency; these indicate softening-type nonlinearity.

It must be observed that the force input around resonance was very distorted with respect to the imposed pure sinusoidal excitation; this is probably the reason for not perfect superposition of part of "up" and "down" responses. Fig. 5(a) shows the harmonic components in the excitation signal for 0.15 N in the frequency range investigated. In particular, the second harmonic of the excitation signal reaches amplitudes much larger than the first harmonic itself, which is the only one controlled. Fortunately in this case higher order harmonics do not have a significant effect on the panel dynamics, as shown by the harmonic components in the response signal shown in Figs. 5(b) for excitation of 0.15 N "up" and "down".

6.2. Nonlinear results for panel B

The nonlinear oscillation amplitude of the panel around the fundamental mode (1, 2) at 125.3 Hz is shown in Fig. 6(a); also in this case, the measured oscillation has been filtered in order to eliminate any frequency except the excitation frequency. The response measurement has been chosen at $x = a/2$, $y = 3/4\,b$, where the vibration amplitude of mode (1,2) is maximum; excitation has been fixed at $\tilde{x} = a/4$, $\tilde{y} = b/4$. In this case, two

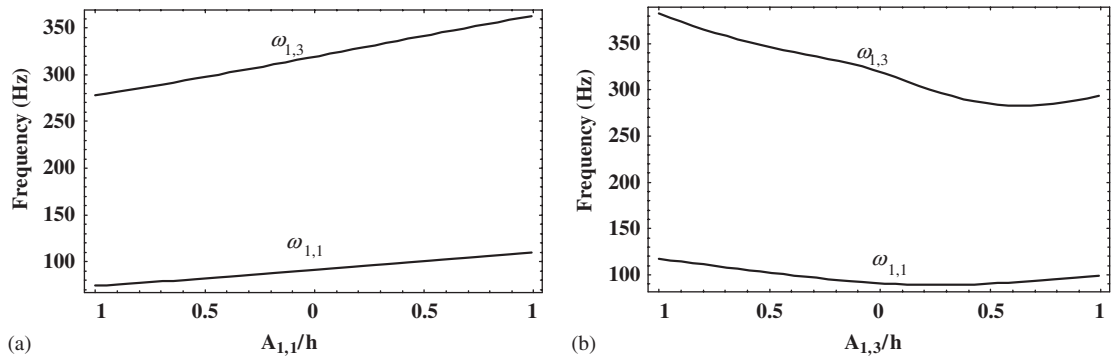

Fig. 8. Natural frequency of modes (1,1) and (1,3) of panel A versus geometric imperfections; 38 dofs model, $k = 0$. (a) Effect of $A_{1,1}$; (b) effect of $A_{1,3}$.

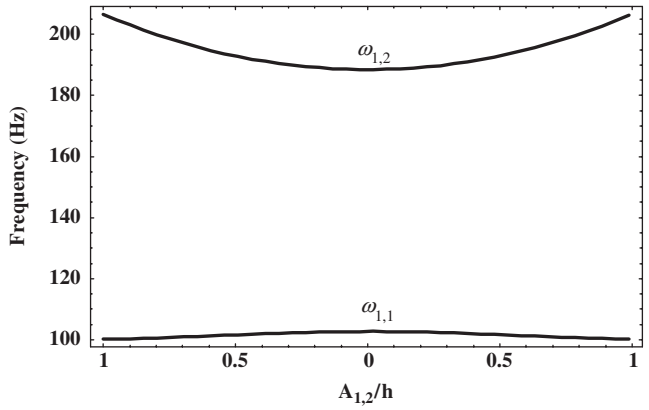

Fig. 9. Natural frequency of modes (1,1) and (1,2) of panel A versus the geometric imperfection $A_{1,2}$; 36 dofs model, $k = 0$.

different force levels have been measured: 0.05, and 0.3 N. The level of 0.05 N gives a very good evaluation of the natural (linear) frequency. For the largest excitation, 0.3 N, softening-type nonlinearity is obtained with jumps. For vibration amplitude of about 1.15 times the plate thickness, the peak of the response appears for a frequency lower of about 5% with respect to the linear one, for the curve at 0.3 N. It must be observed that the second natural frequency of the panel is for mode (1,1) at 142.2 Hz.

The harmonic components of the excitation and response at 0.3 N are given in Figs. 6(b)–(e); here the mean value has not been measured, as a consequence of "AC coupling" setting of the front-end during experiments.

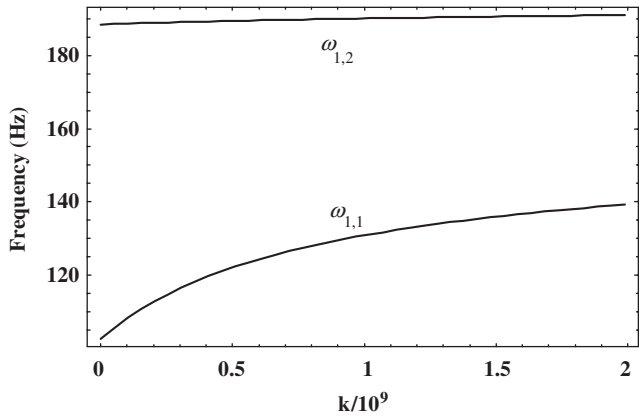

Fig. 10. Natural frequency of modes (1,1) and (1,2) of panel perfect A versus the stiffness k (N/m^2) of in-plane, tangential distributed springs; 36 dofs model.

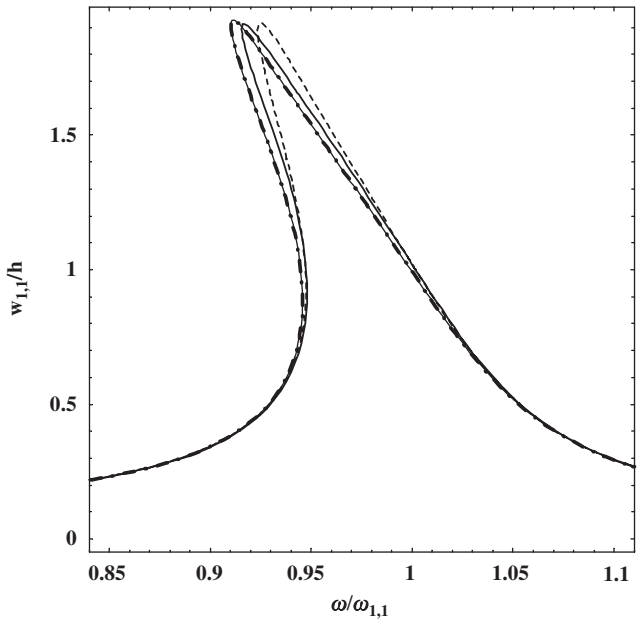

Fig. 11. Convergence of models for nonlinear forced vibrations of perfect panel A; first-harmonic component of the non-dimensional response versus non-dimensional excitation frequency; fundamental mode (1,1), $f = 0.0632$, $\zeta_{1,1} = 0.0177$ and $k = 0$. --, 13 dofs, —, 24 dofs, —, 36 dofs, –––, 38 dofs.

7. Theoretical results and comparison to experiments

7.1. Panel A, mode (1,1)

The effect of geometric imperfections $A_{1,1}$, $A_{1,2}$ and $A_{1,3}$ on the natural frequency of mode (1,1) is shown in Figs. 7(a)–(c), respectively, for $k = 0$ with a 13 dofs model including the following generalized coordinates: $w_{1,1}$, $u_{1,0}$, $u_{1,2}$, $u_{1,4}$, $u_{3,0}$, $u_{3,2}$, $u_{3,4}$, $v_{0,1}$, $v_{2,1}$, $v_{4,1}$, $v_{0,3}$, $v_{2,3}$, $v_{4,3}$. It can be observed that many in-plane generalized coordinates must be used in order to obtain good accuracy of the model; in this case, only one transverse coordinate is used versus 12 in-plane coodinates; similar results have been found for plates and shells of different geometry [24]. The geometric imperfection $A_{1,1}$ has the same shape of the fundamental mode (1,1) in transverse direction, but it is associated with zero in-plane imperfection. Results show that geometric imperfections of the order of the panel thickness give a large change to the fundamental frequency. However, these results cannot be considered accurate because the 13 dofs model is not yet at convergence for linear results. In particular, the effect of imperfection $A_{1,2}$ is very poorly evaluated. For this reason more accurate models, with larger dofs, have been used.

The effects of geometric imperfections $A_{1,1}$ and $A_{1,3}$ on the natural frequency of modes (1,1) and (1,3) are shown in Figs. 8(a) and (b), respectively; results have been obtained for $k = 0$ with a 38 dofs model including the following generalized coordinates: $w_{1,1}$, $w_{1,3}$, $w_{3,1}$, $w_{3,3}$, $w_{1,5}$, $w_{5,1}$, $u_{1,0}$, $u_{1,2}$, $u_{1,4}$, $u_{1,6}$, $u_{1,8}$, $u_{1,10}$, $u_{1,12}$, $u_{1,14}$, $u_{1,16}$, $u_{1,18}$, $u_{1,20}$, $u_{3,0}$, $u_{3,2}$, $u_{3,4}$, $u_{3,6}$, $u_{3,8}$, $v_{0,1}$, $v_{2,1}$, $v_{4,1}$, $v_{6,1}$, $v_{8,1}$, $v_{10,1}$, $v_{12,1}$, $v_{14,1}$, $v_{16,1}$, $v_{18,1}$, $v_{20,1}$, $v_{0,3}$, $v_{2,3}$, $v_{4,3}$, $v_{6,3}$, $v_{8,3}$. The effect of imperfection $A_{1,2}$ on the natural frequencies of modes (1,1) and (1,2) is presented in Fig. 9, obtained for $k = 0$ with a 36 dofs model including: $w_{1,2}$, $w_{1,1}$, $w_{1,3}$, $w_{3,1}$, $w_{3,3}$, $w_{1,4}$, $u_{1,1}$, $u_{1,3}$, $u_{1,5}$, $u_{3,1}$, $u_{3,3}$, $u_{3,5}$, $u_{1,0}$, $u_{1,2}$, $u_{1,4}$, $u_{3,0}$, $u_{3,2}$, $u_{3,4}$, $u_{5,0}$, $u_{5,2}$, $u_{5,4}$, $v_{0,2}$, $v_{2,2}$, $v_{4,2}$, $v_{0,4}$, $v_{2,4}$, $v_{4,4}$, $v_{0,1}$, $v_{2,1}$, $v_{4,1}$, $v_{0,3}$, $v_{2,3}$, $v_{4,3}$, $v_{0,5}$, $v_{2,5}$, $v_{4,5}$. Comparing Figs. 9 and 7(b) it is clearly understood that the 13 dofs model is not suitable for evaluating the effect of imperfection $A_{1,2}$.

The effect of the stiffness k (N/m^2) of distributed springs parallel to the panel edges on natural frequencies of modes (1,1) and (1,2) is shown in Fig. 10, obtained for perfect panel with the 36 dofs model previously described. Fig. 10 shows that k larger than 2×10^9 N/m^2 is necessary to simulate classical simply supported panel.

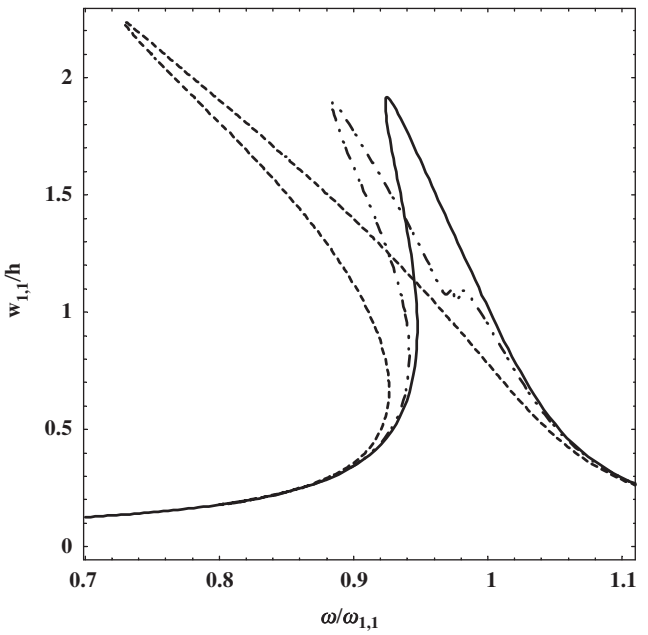

Fig. 12. First-harmonic component of the non-dimensional response of the perfect panel A with different boundary conditions versus non-dimensional excitation frequency; mode (1,1), $f = 0.0632$, $\zeta_{1,1} = 0.0177$ and $k = 0$. ----, classical simply supported panel, 9 dofs; model developed in [17]; – – –, present model with $k = 2 \times 10^8$ N/m^2, 36 dofs; —, present model with $k = 0$, 13 dofs.

After this linear study, forced vibrations of large amplitude are studied by using the software AUTO 97. The following non-dimensional modal excitation on the generalized coordinate $w_{1,1}$ is introduced and its amplitude is immediately related to the point force excitation $\tilde{f}$ at $(x = \tilde{x},\ y = \tilde{y})$

$$f = \frac{\tilde{f}\,\sin(\pi\tilde{x}/a)\,\sin(\pi\tilde{y}/a)}{h^2\rho_S\omega_{1,1}^2(a/2)(b/2)}.$$

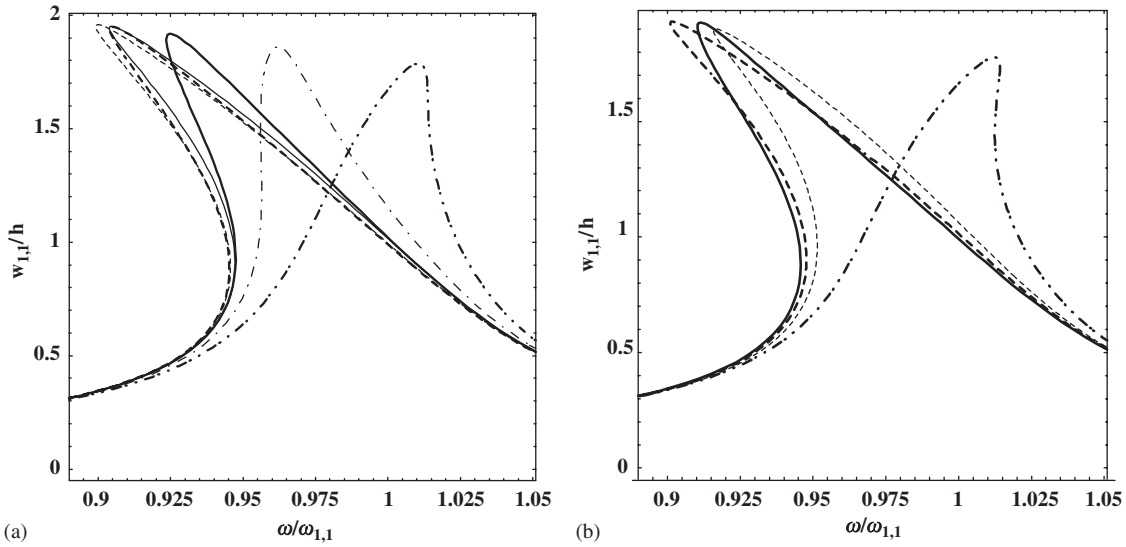

Fig. 13. Effect of geometric imperfection $A_{1,1}$ on the first-harmonic component of the non-dimensional response of panel A versus non-dimensional excitation frequency; mode (1,1), $f = 0.0632$, $\zeta_{1,1} = 0.0177$ and $k = 0$. —, $A_{1,1} = 0$; - -, $A_{1,1} = 0.5h$; – –, $A_{1,1} = h$; —, $A_{1,1} = 1.5h$; – - –, $A_{1,1} = -0.5h$; – - –, $A_{1,1} = -h$. (a) 13 dofs model and (b) 38 dofs model.

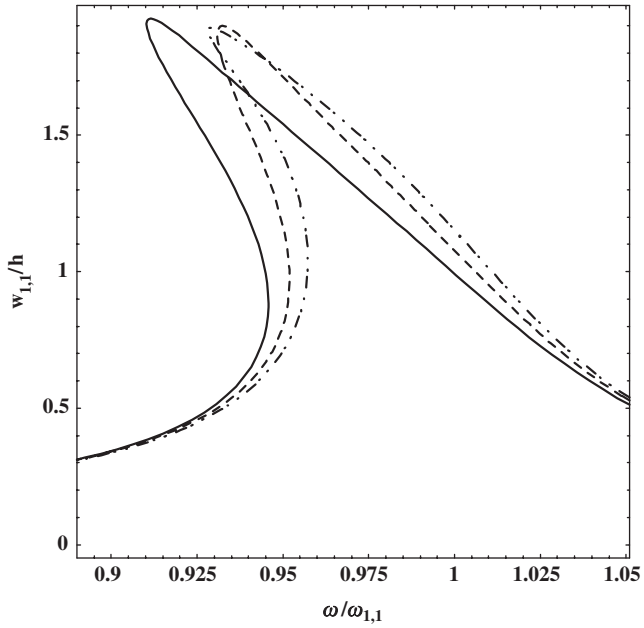

Fig. 14. Effect of geometric imperfection $A_{1,3}$ on the first-harmonic component of the non-dimensional response of panel A versus non-dimensional excitation frequency; mode (1,1), $f = 0.0632$, $\zeta_{1,1} = 0.0177$, $k = 0, 38$ dofs. —, $A_{1,3} = 0$; - -, $A_{1,3} = 0.3h$; – - –, $A_{1,3} = -0.3h$.

Harmonic excitation of non-dimensional amplitude $f = 0.0632$ (chosen in order to reach large-amplitude vibrations) has been imposed in the frequency range around the resonance of the fundamental mode (1,1). The convergence of the solution, for different numbers of generalized coordinates retained in the expansion, is shown in Fig. 11 for perfect panel with $k = 0$. In particular, four models are compared: 13, 24, 36 and 38 dofs; the 24 dofs model has (the others have already been described): $w_{1,1}$, $w_{1,3}$, $w_{3,1}$, $w_{3,3}$, $u_{1,0}$, $u_{1,2}$, $u_{1,4}$, $u_{1,6}$, $u_{1,8}$,

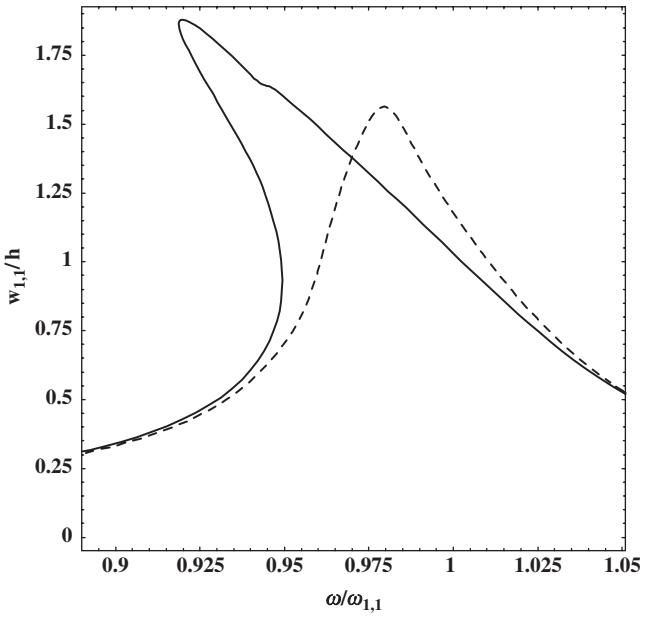

Fig. 15. Effect of geometric imperfection $A_{1,2}$ on the first-harmonic component of the non-dimensional response of panel A versus non-dimensional excitation frequency; mode (1,1), $f = 0.0632$, $\zeta_{1,1} = 0.0177$, $k = 0, 36$ dofs. —, $A_{1,3} = 0$; - -, $A_{1,3} = 0.5h$.

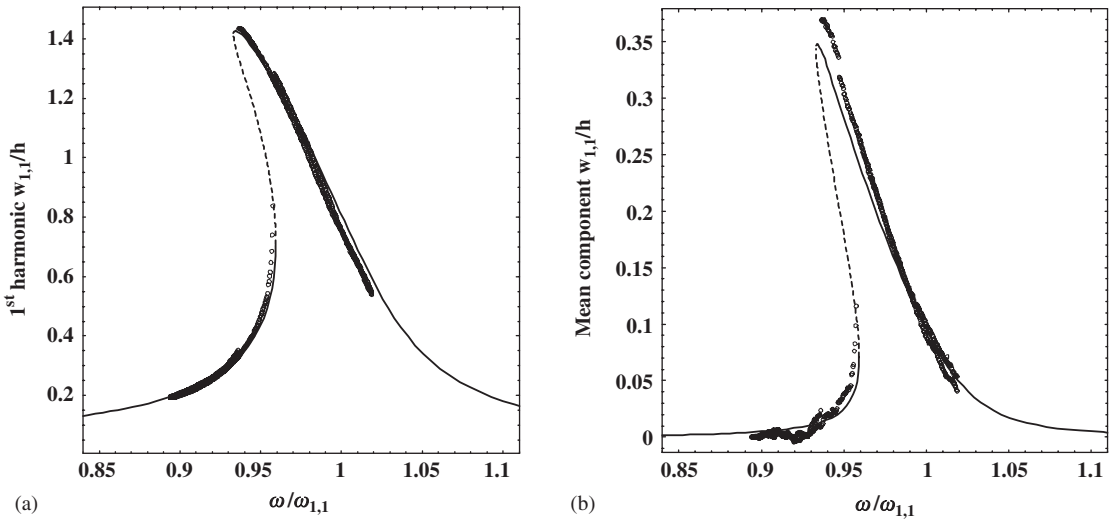

Fig. 16. Comparison of numerical and experimental results for the non-dimensional response of panel A versus non-dimensional excitation frequency; mode (1,1), $\tilde{f} = 0.15$ N, $\zeta_{1,1} = 0.012$, $A_{1,1} = 0.35h$; $k = 2 \times 10^8$ N/m^2, 36 dofs. ○, experimental data, —, stable theoretical solutions, − − −, unstable theoretical solutions. (a) First harmonic and (b) mean value.

$u_{3,0}$, $u_{3,2}$, $u_{3,4}$, $u_{3,6}$, $u_{3,8}$, $v_{0,1}$, $v_{2,1}$, $v_{4,1}$, $v_{6,1}$, $v_{8,1}$, $v_{0,3}$, $v_{2,3}$, $v_{4,3}$, $v_{6,3}$, $v_{8,3}$. All of them give very close results showing softening type nonlinearity, with the most accurate being the 36 and 38 dofs which give coincident curves. In Fig. 11, only the generalized coordinate $w_{1,1}$ has been plotted, which practically coincides with the panel oscillation at the center, as it will be shown shortly in this section. Moreover, only the first harmonic of $w_{1,1}$ has been plotted; super-harmonics in $w_{1,1}$ are negligible, as it will be shown shortly, but a zero-frequency component (mean value) is significant, giving rise to larger oscillation inwards than outwards, with respect to the center of curvature of the panel.

Fig. 12 shows the effect of the boundary conditions on the nonlinear response of the perfect panel. In fact three different boundary conditions are compared: classical simply supported (see Ref. [17] where this boundary condition has been studied) versus the present model for $k = 0$ and$2 \times 10^8\,\mathrm{N/m^2}$. The simply supported panel for mode (1,1) presents a significantly enhanced softening nonlinearity with respect to the present model with free in-plane edges ($k = 0$), while the case for $k = 2 \times 10^8\,\mathrm{N/m^2}$ obviously lies in between.

The effect of geometric imperfection $A_{1,1}$ on nonlinear response of mode (1,1) is investigated in Figs. 13 (a, b) for the 13 and 38 dofs models. According to the 13 dofs model, the response with the strongest softening nonlinearity is obtained for $A_{1,1} = h$, while for the 38 dofs model for $A_{1,1} = 0.5\,h$. Both models show that small imperfection $A_{1,1}$ enhances the nonlinearity, and then reduces it for amplitudes of the order of h or larger; negative $A_{1,1}$ give rise to hardening type nonlinearity. The effect of imperfection $A_{1,3}$ is analysed only for the 38 dofs model in Fig. 14. Both positive and negative values reduces the nonlinearity. Finally the effect of $A_{1,2}$ is investigated in Fig. 15 on the 36 dofs model; also in this case imperfections reduce the nonlinearity.

A comparison of theoretical (36 dofs model with $k = 3 \times 10^8\,\mathrm{N/m^2}$) and experimental results for excitation $\tilde{f}$ =0.15 N at ($\tilde{x} = a/4$, $\tilde{y} = b/3$) is shown in Fig. 16 (damping $\zeta_{1,1} = 0.012$, assumed to be the same for all the generalized coordinates). Comparison of numerical and experimental results is excellent for both the first harmonic and the mean value. Calculations have been obtained introducing the geometric imperfection $A_{1,1} = 0.35\,h$, having the form of mode (1,1), which is of the same order of magnitude of measured imperfections of the plate surface, as reported in Fig. 3. While the first harmonic of the response is the most significant one because it is directly excited, the mean value (constant value, at zero-frequency) of the response indicates an asymmetric oscillation of the panel inwards and outwards. Additional harmonics of the response are much smaller, as shown in Fig. 5(b). The assumed value of $k = 3 \times 10^8\,\mathrm{N/m^2}$ is compatible with the

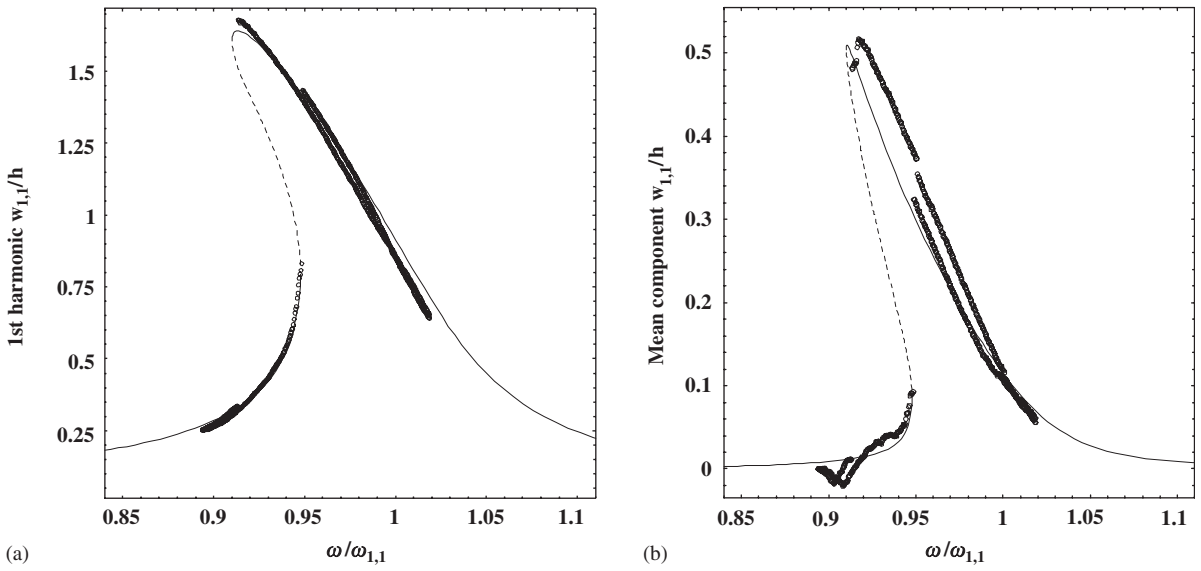

Fig. 17. Comparison of numerical and experimental results for the non-dimensional response of panel A versus non-dimensional excitation frequency; mode (1,1), $\tilde{f} = 0.2$ N, $\zeta_{1,1} = 0.011$, $A_{1,1} = 0.35h$; $k = 2 \times 10^8\,\mathrm{N/m^2}$, 36 dofs. ○, experimental data; —, stable theoretical solutions; − − −, unstable theoretical solutions. (a) First harmonic and (b) mean value.

experimental boundary condition; the value of damping has been identified by using the nonlinear experimental response.

A second comparison of theoretical and experimental results is shown in Fig. 17 for excitation $\tilde{f}$ =0.2 N (damping $\zeta_{1,1} = 0.011$). This comparison is also excellent for both the 1st harmonic and the mean value. In Figs. 16 and 17 the indication of stability of the solution is also given; however, it is the classical one of system with softening-type nonlinearity. The value of damping has been identified by using the nonlinear experimental response also in this case and shows a slightly increased damping with the increased excitation; the presence of nonlinear damping, generally increasing with the amplitude of oscillation, has been previously observed and discussed by the author on experiments on a complete circular cylindrical shell [25].

The five main generalized coordinates associated to the panel response given in Fig. 16 are reported in Fig. 18 for completeness. In particular, the asymmetry of the response of $w_{1,1}$ shows large difference between

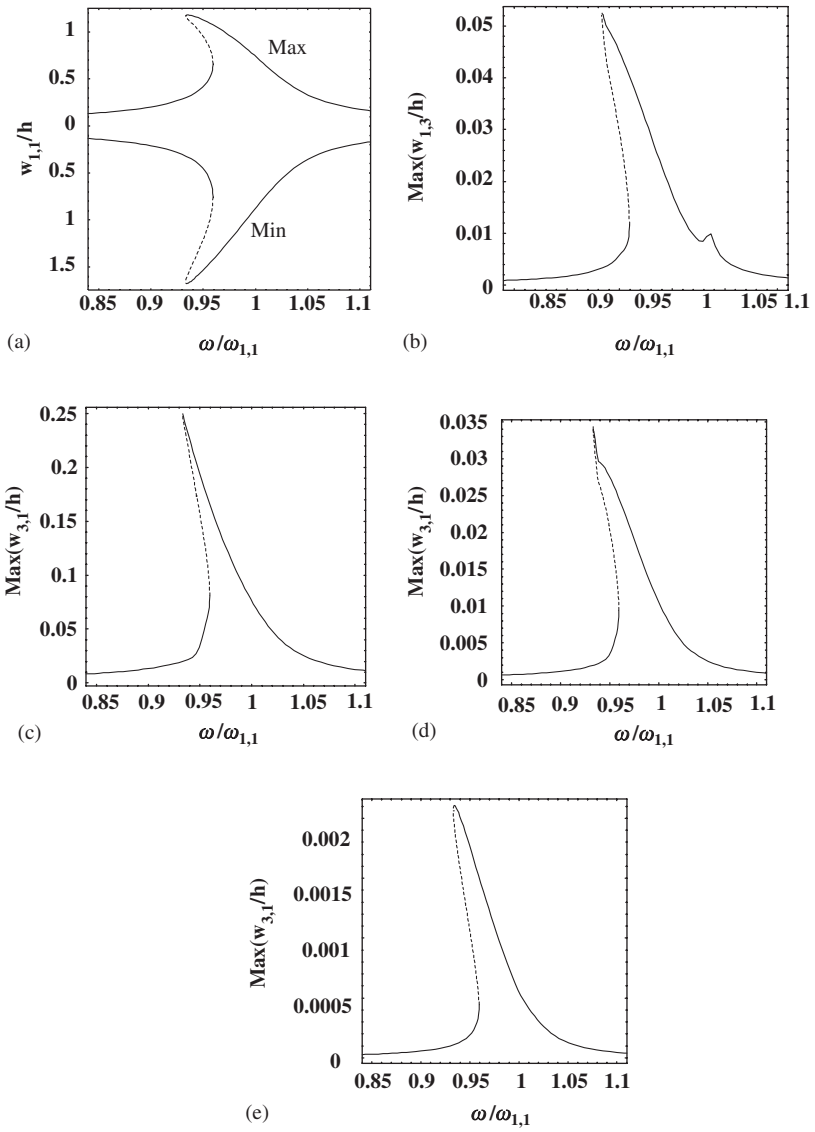

Fig. 18. Response of panel A; fundamental mode (1,1), $\tilde{f} = 0.15$ N, $\zeta_{1,1} = 0.012$, $A_{1,1} = 0.35h$; $k = 2 \times 10^8$ N/m^2, 36 dofs. —, stable periodic response; - - - -, unstable periodic response. (a) Maximum and minimum of the generalized coordinate $w_{1,1}$; (b) maximum of the generalized coordinate $w_{1,3}$; (c) maximum of the generalized coordinate $w_{3,1}$; (d) maximum of the generalized coordinate $w_{3,3}$; and (e) maximum of the generalized coordinate $u_{1,0}$.

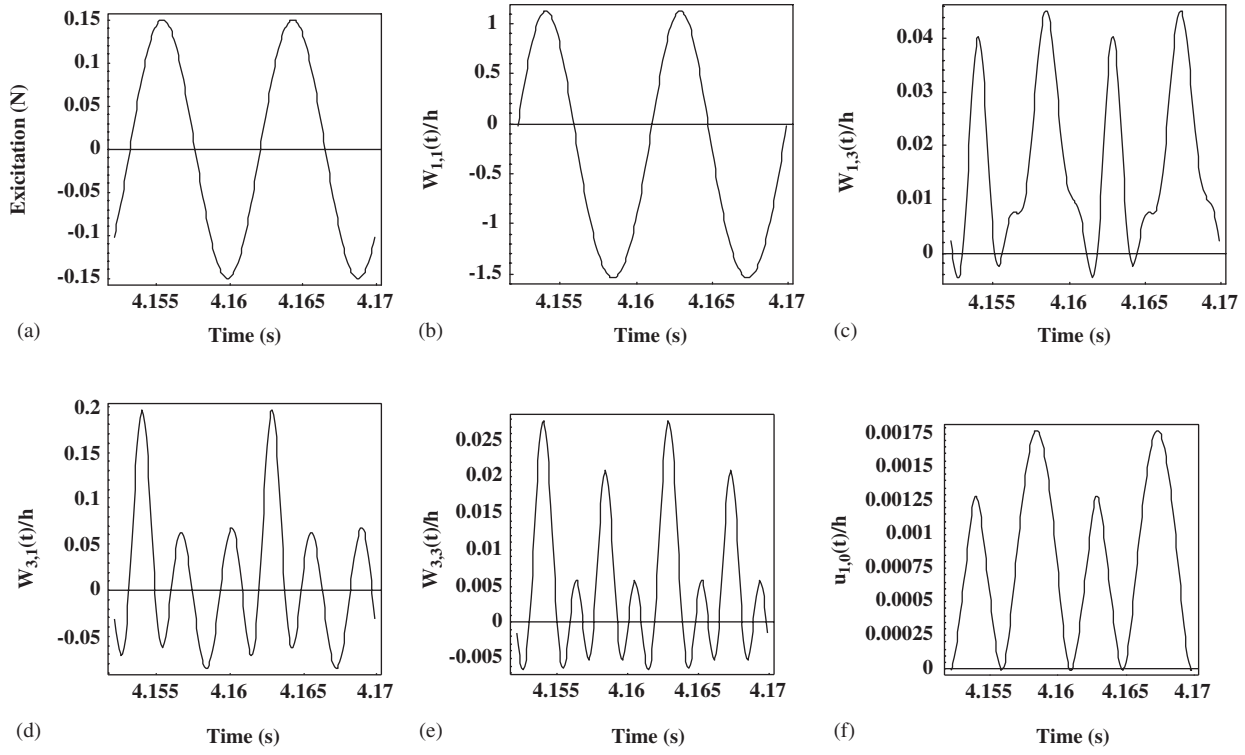

Fig. 19. Computed time response of the panel A for excitation frequency $\omega = 0.95\omega_{1,1}$; fundamental mode (1,1), $\tilde{f} = 0.15$ N, $\zeta_{1,1} = 0.012$, $A_{1,1} = 0.35h$; $k = 2 \times 10^8$ N/m^2, 36 dofs. (a) Force excitation; (b) generalized coordinate $w_{1,1}$; (c) generalized coordinate $w_{1,3}$; (d) generalized coordinate $w_{3,1}$; (e) generalized coordinate $w_{3,3}$; and (f) generalized coordinate $u_{1,0}$.

maximum (outwards) and minimum (inwards) oscillation, giving rise to the mean value of the response previously shown. This behaviour is investigated with more accuracy in Fig. 19, where the time response have been plotted for excitation frequency $\omega = 0.95\omega_{1,1}$, i.e. close to the peak of the response; these results have been obtained by direct integration of the equations of motion by using the DIVPAG routine of the Fortran library IMSL, while all the previous ones have been obtained by using AUTO 97. Fig. 19 also indicates the phase relationship with respect to the excitation. The presence of super-harmonics and zero-frequency (mean value) component is clarified in Fig. 20 with the frequency spectra.

7.2. Panel B, mode (1,2)

The effect of geometric imperfections $A_{1,1}$, $A_{1,2}$ and $A_{1,4}$ on the natural frequency of modes (1,1) and (1,2) is shown in Figs. 21(a–c), respectively, for $k = 0$ with a 36 dofs model including the following generalized coordinates: $w_{1,2}$, $w_{1,1}$, $w_{1,3}$, $w_{3,1}$, $w_{3,3}$, $w_{1,4}$, $u_{1,1}$, $u_{1,3}$, $u_{1,5}$, $u_{3,1}$, $u_{3,3}$, $u_{3,5}$, $u_{1,0}$, $u_{1,2}$, $u_{1,4}$, $u_{3,0}$, $u_{3,2}$, $u_{3,4}$, $u_{5,0}$, $u_{5,2}$, $u_{5,4}$, $v_{0,2}$, $v_{2,2}$, $v_{4,2}$, $v_{0,4}$, $v_{2,4}$, $v_{4,4}$, $v_{0,1}$, $v_{2,1}$, $v_{4,1}$, $v_{0,3}$, $v_{2,3}$, $v_{4,3}$, $v_{0,5}$, $v_{2,5}$, $v_{4,5}$, i.e. the same ones used in the 36 dofs model for panel A. Also in this case, results show that geometric imperfection of the order of the panel thickness give a large change of the fundamental frequency. Here the natural frequencies of modes (1,1) and (1,2) are very close for zero imperfection.

The effect of the stiffness k (N/m^2) of distributed springs parallel to the panel edges on natural frequencies of modes (1,2) and (1,1) is shown in Fig. 22(a, b), obtained for perfect panel with the 36 dofs model previously described. Fig. 22(a) shows that k equal or larger than 0.8×10^{10} N/m^2 is necessary to simulate classical simply supported panel. Fig. 22(b) is a zoom of Fig. 22(a) in order to show the behaviour for small spring stiffness; it is evident that the fundamental mode is (1,1) for $k = 0$, but at $k = 0.05 \times 10^8$ N/m^2 the curves cross each other, and after mode (1,2) becomes the fundamental mode of the panel.

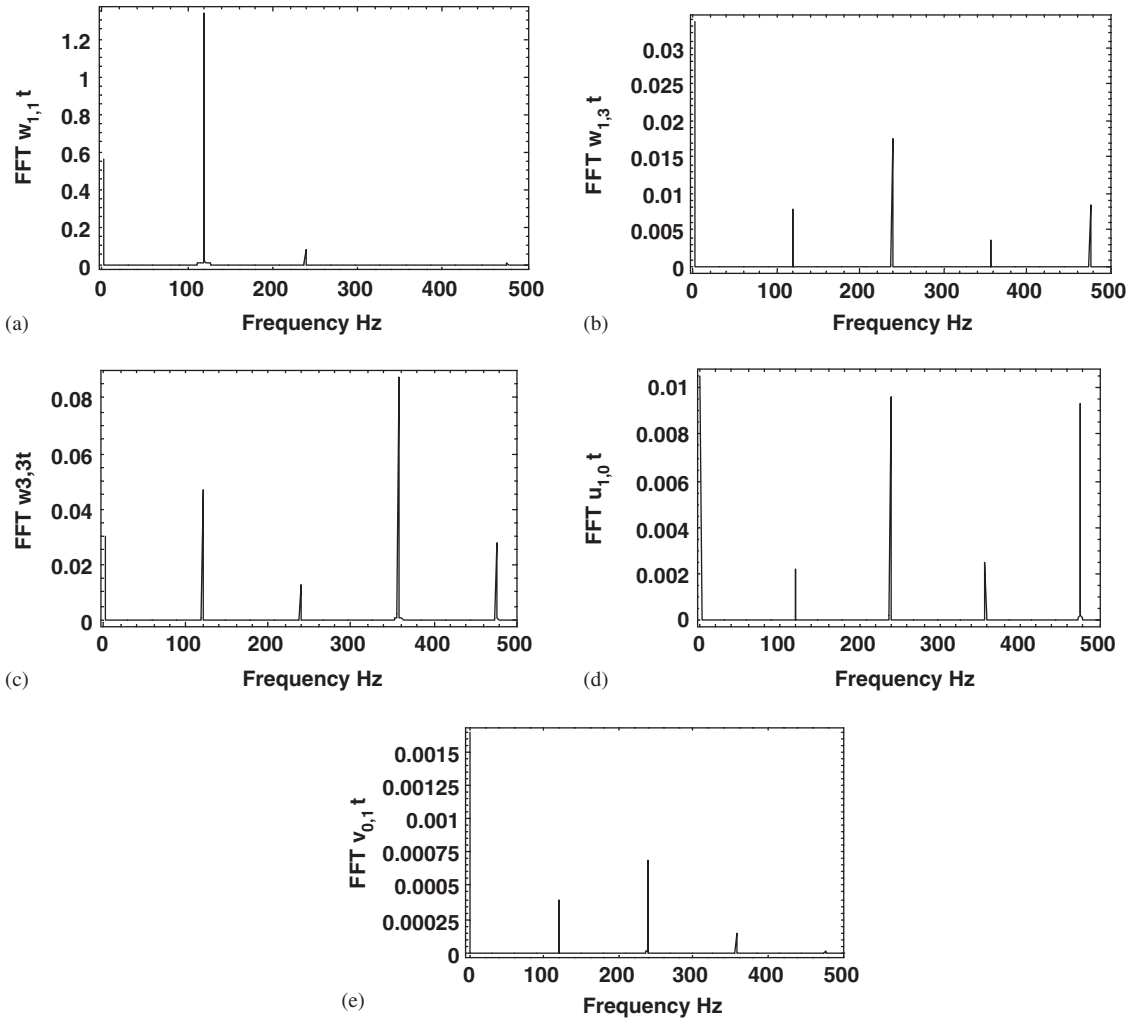

Fig. 20. Frequency spectrum of the response of the panel A for excitation frequency $\omega = 0.95\omega_{1,1}$; fundamental mode (1,1), $\tilde{f} = 0.15$ N, $\zeta_{1,1} = 0.012$, $A_{1,1} = 0.35h$; $k = 2 \times 10^8$ N/m^2, 36 dofs. (a) Generalized coordinate $w_{1,1}$; (b) generalized coordinate $w_{1,3}$; (c) generalized coordinate $w_{3,1}$; (d) generalized coordinate $w_{3,3}$; and (e) generalized coordinate $u_{1,0}$.

In order to study the nonlinear response, harmonic excitation has been applied to the generalized coordinate $w_{1,2}$ only (modal excitation) corresponding to a force $\tilde{f}$ =0.3 N at $\tilde{x} = a/4$ and $\tilde{y} = b/4$ ($f = 0.0366$) in the frequency range around resonance of the fundamental mode (1, 2). The convergence of the solution, for different numbers of generalized coordinates retained in the expansion, is shown in Fig. 23 for perfect panel with $k = 0$. In particular, three models are compared: 26, 30 and 36 dofs; the 26 dofs model has: $w_{1,2}$, $w_{1,1}$, $w_{1,3}$, $w_{3,1}$, $w_{3,2}$, $u_{1,1}$, $u_{1,3}$, $u_{1,5}$, $u_{3,1}$, $u_{3,3}$, $u_{3,5}$, $u_{1,0}$, $u_{1,2}$, $u_{1,4}$, $u_{3,0}$, $u_{3,2}$, $u_{3,4}$, $v_{0,2}$, $v_{2,2}$, $v_{4,2}$, $v_{0,1}$, $v_{2,1}$, $v_{4,1}$, $v_{0,3}$, $v_{2,3}$, $v_{4,3}$. The 30 dofs model has: $w_{1,2}$, $w_{1,1}$, $w_{1,3}$, $w_{3,1}$, $w_{3,3}$, $u_{1,1}$, $u_{1,3}$, $u_{1,5}$, $u_{3,1}$, $u_{3,3}$, $u_{3,5}$, $u_{1,0}$, $u_{1,2}$, $u_{1,4}$, $u_{3,0}$, $u_{3,2}$, $u_{3,4}$, $u_{5,0}$, $u_{5,2}$, $u_{5,4}$, $v_{0,2}$, $v_{2,2}$, $v_{4,2}$, $v_{0,1}$, $v_{2,1}$, $v_{4,1}$, $v_{0,3}$, $v_{2,3}$, $v_{4,3}$, $v_{0,5}$, $v_{2,5}$, $v_{4,5}$. Differently with respect to panel A, where mode (1,1) was investigated, here the choice of the generalized coordinates to be inserted in the model is much more complicated, and only the 36 dofs model is accurate. In fact, the presence of the generalized coordinate $w_{1,4}$ has been found to be fundamental to reach the required accuracy. In Fig. 23 only the generalized coordinate $w_{1,2}$ has been plotted, which practically coincides with the panel peak oscillation, which is at $x = a/2$, $y = 3/4\,b$. Here the maximum value of $w_{1,2}$ has been plotted, which is coincident with the value of the first harmonic; super-harmonics and zero frequency component in $w_{1,2}$ are

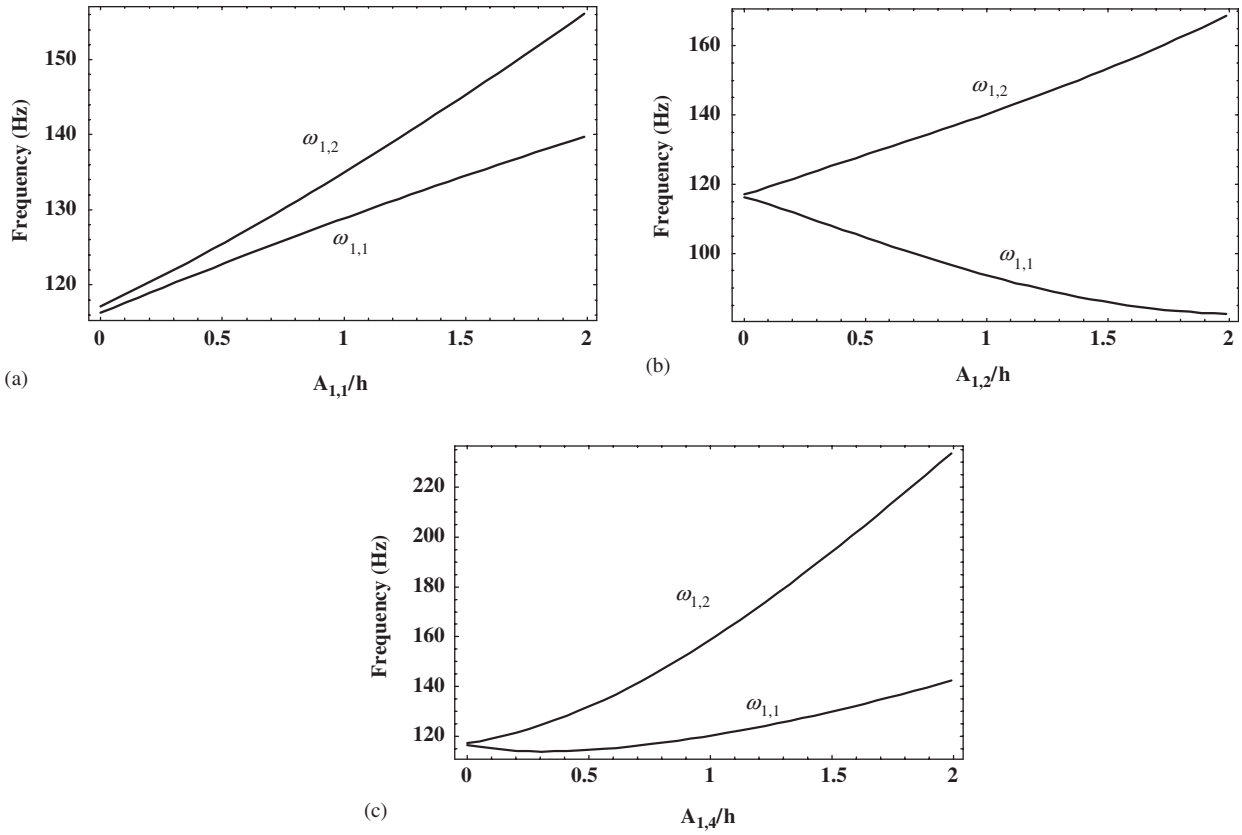

Fig. 21. Natural frequency of modes (1,2) and (1,1) of panel B versus geometric imperfections; 36 dofs model, $k = 0$. (a) Effect of $A_{1,1}$; (b) effect of $A_{1,2}$; and (c) effect of $A_{1,4}$.

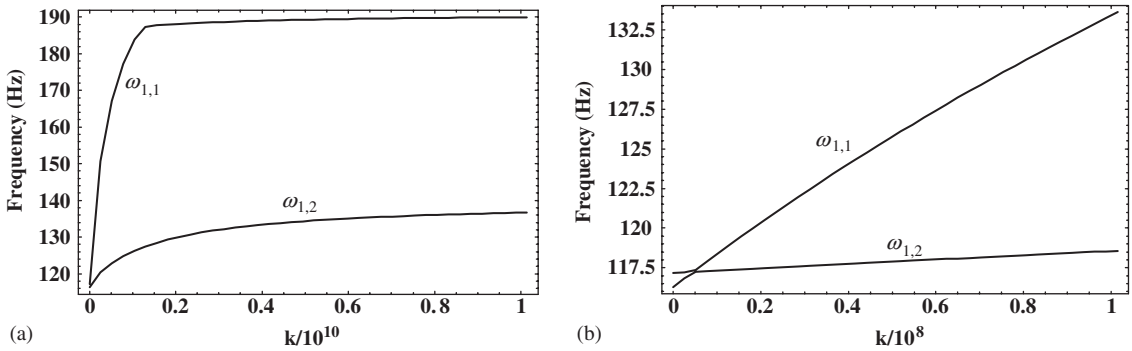

Fig. 22. Natural frequency of modes (1,1) and (1,2) of perfect panel B versus the stiffness k (N/m^2) of in-plane, tangential distributed springs; 36 dofs model. (a) Full plot and (b) close-up plot of the origin.

zero, as it will be shown shortly. The computer program AUTO 97 has been used to study the nonlinear equations of motion.

Fig. 24 shows the effect of the boundary conditions on the nonlinear response of mode (1,2) of the perfect panel. In fact, three different boundary conditions are compared: classical simply supported (see Ref. [17]) versus the present model for $k = 0$ and 5×10^8 N/m^2. The simply supported panel for mode (1,2) presents a strong hardening-type nonlinearity whereas the present model with free in-plane edges ($k = 0$) has softening-type nonlinearity; the case for $k = 5 \times 10^8$ N/m^2 obviously lies in between, with a very weak softening-type

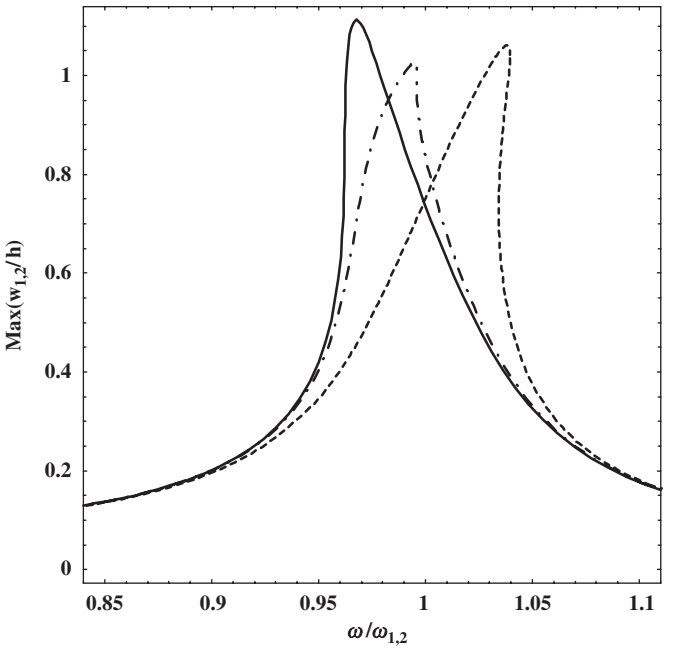

Fig. 23. Convergence of models for nonlinear forced vibrations of perfect panel B; maximum of $w_{1,2}$ (coincident with its first-harmonic) versus non-dimensional excitation frequency; mode (1,2), $f = 0.0366$, $\zeta_{1,2} = 0.0162$ and $k = 0$. —, 36 dofs; – – –, 30 dofs; - -, 26 dofs.

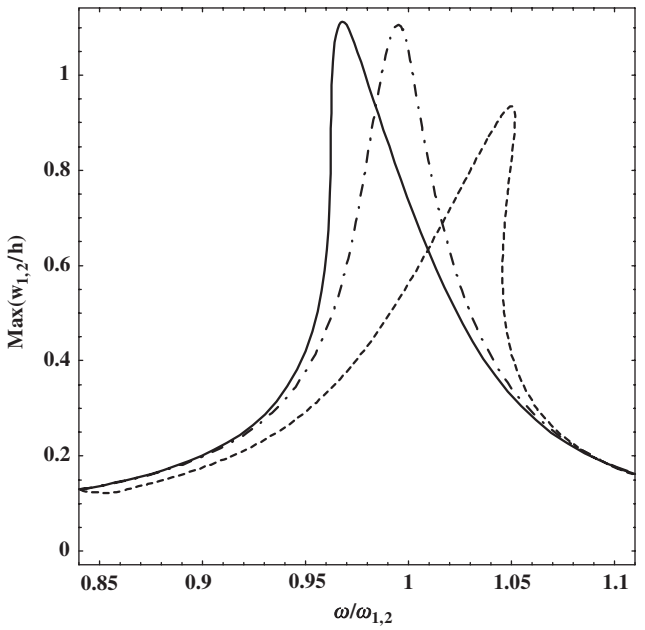

Fig. 24. Non-dimensional response $w_{1,2}$ of the perfect panel B with different boundary conditions versus non-dimensional excitation frequency; mode (1,2), $f = 0.0366$, $\zeta_{1,2} = 0.0162$ and $k = 0$. - -, classical simply supported panel, 36 dofs, [17]; – – –, present model with $k = 5 \times 10^8$ N/m^2, 36 dofs; —, present model with $k = 0$, 36 dofs.

nonlinearity. This result is completely different with respect to the result found for mode (1,1) of panel A; difference is due to the different mode studied. The simply supported model has 36 dofs: $w_{1,2}$, $w_{1,1}$, $w_{1,3}$, $w_{3,1}$, $w_{3,3}$, $w_{1,4}$, $u_{1,1}$, $u_{1,2}$, $u_{1,3}$, $u_{1,4}$, $u_{1,5}$, $u_{3,1}$, $u_{3,2}$, $u_{3,3}$, $u_{3,4}$, $u_{3,5}$, $u_{5,1}$, $u_{5,2}$, $u_{5,3}$, $u_{5,4}$, $u_{5,5}$, $v_{1,1}$, $v_{1,2}$, $v_{1,3}$, $v_{1,4}$, $v_{1,5}$, $v_{3,1}$, $v_{3,2}$,

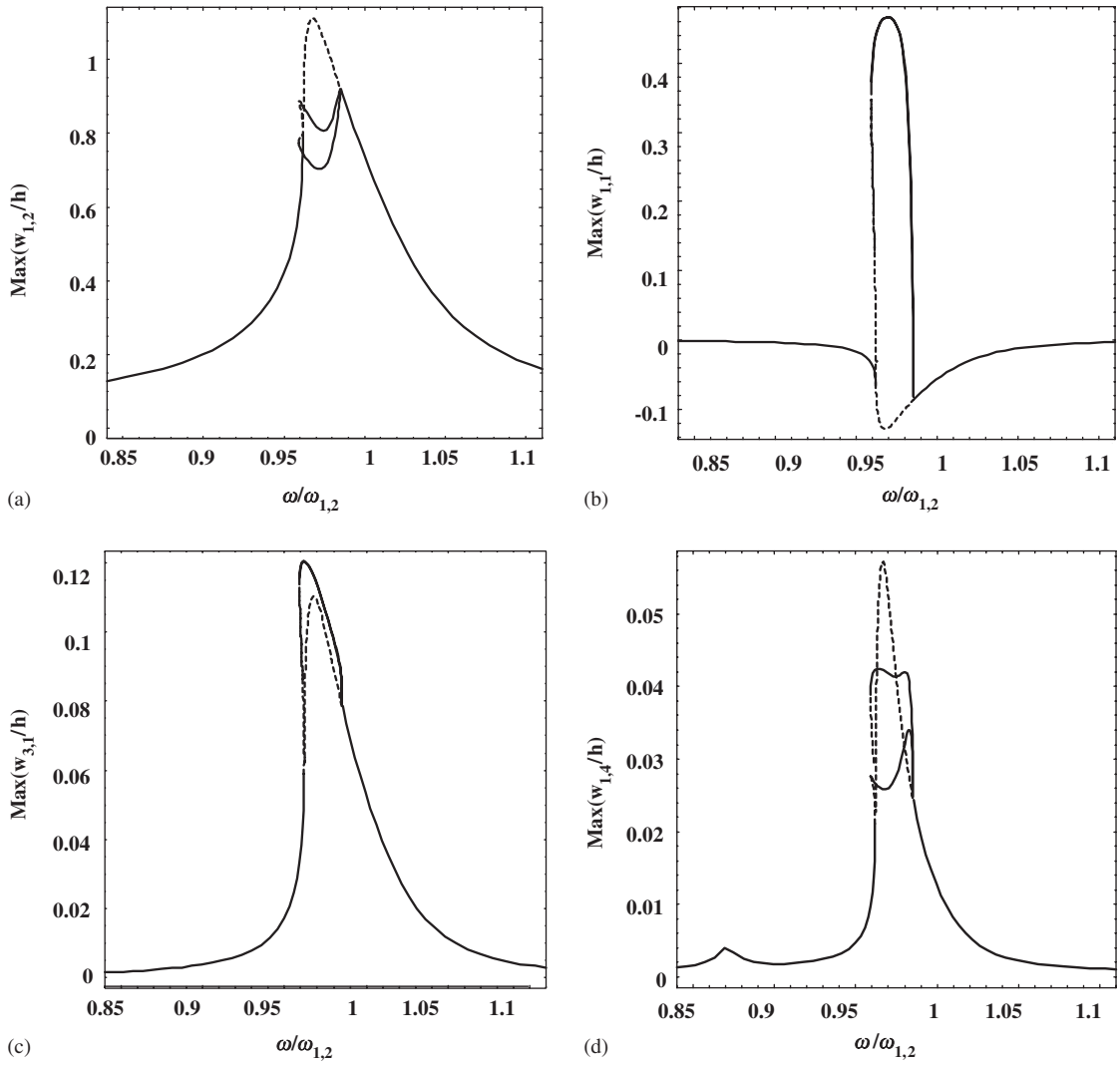

Fig. 25. One-to-one internal resonance: non-dimensional response of the perfect panel B versus non-dimensional excitation frequency; excitation on mode (1,2), $f = 0.0366$, $\zeta_{1,2} = 0.0162$ and $k = 0$; 36 dofs. —, stable periodic response; - -, unstable periodic response. (a) Generalized coordinate $w_{1,2}$; (b) generalized coordinate $w_{1,1}$; (c) generalized coordinate $w_{3,1}$; and (d) generalized coordinate $w_{1,4}$.

$v_{3,3}$, $v_{3,4}$, $v_{3,5}$, $v_{5,1}$, $v_{5,2}$, $v_{5,3}$, $v_{5,4}$, $v_{5,5}$. It must be observed that numerical results for higher modes than (1,1) are very scarce in the literature and indicates hardening-type nonlinearity [18]. The present results for mode (1,2) are fundamental because they explain for the first time the role of in-plane tangential boundary conditions on the nonlinearity of the panel.

A very interesting one-to-one internal resonance is observed for the perfect panel with $k = 0$. In fact, the main branch bifurcates (pitchfork bifurcation) close to the peak of the response of $w_{1,2}$ and gives rise to a second branch, which is stable, as shown in Fig. 25. This internal resonance between modes (1,2) and (1,1) is due to the fact that $\omega_{1,2} = 117.2$ Hz and $\omega_{1,1} = 116.3$ Hz are extremely close in this case. Therefore around the resonance of mode (1,2), which is the only one directly excited, energy is transferred to mode (1,1) as shown in Fig. 25(b). Therefore the peak of the response of $w_{1,2}$ is cut as indicated in Fig. 25(a). Other significant generalized coordinates are shown in Figs. 25(c,d). A one-to-one resonance is always present in complete, perfect, circular cylindrical shells [21,25], where an energy transfer from the driven mode to the companion mode is observed. In fact, the type of one-to-one resonance obtained for a complete circular cylindrical shell is

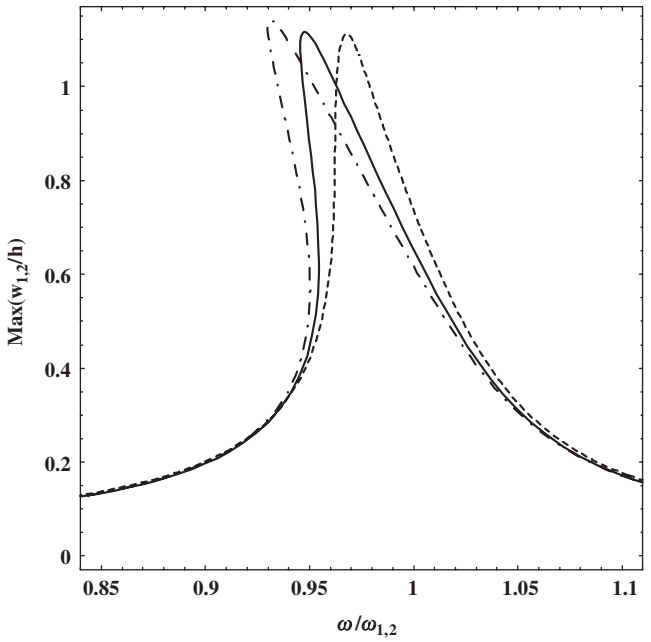

Fig. 26. Effect of geometric imperfection $A_{1,1}$ on the non-dimensional response $w_{1,2}$ of panel B versus non-dimensional excitation frequency; mode (1,2), $f = 0.0366$, $\zeta_{1,2} = 0.0162$ and $k = 0$; 36 dofs. --, $A_{1,1} = 0$; —, $A_{1,1} = 0.7h$; – – –, $A_{1,1} = 1.5h$.

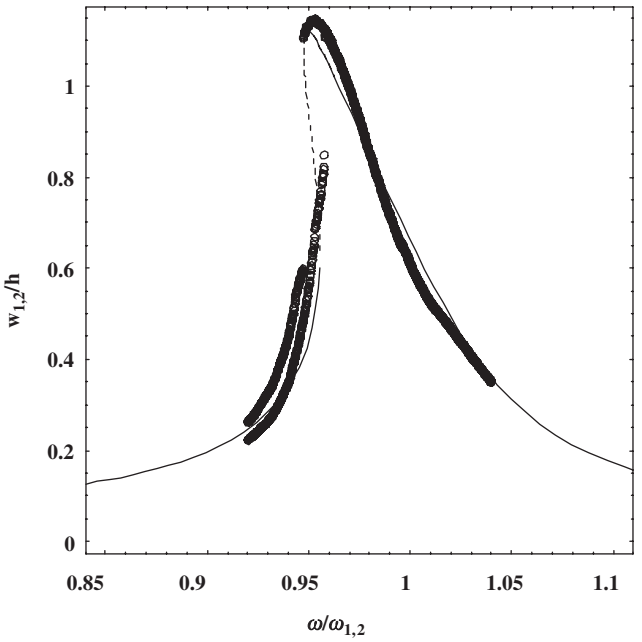

Fig. 27. Comparison of numerical and experimental results for the non-dimensional response of panel B versus non-dimensional excitation frequency; mode (1,2), $\tilde{f} = 0.3$ N, $\zeta_{1,2} = 0.0162$, $A_{1,1} = 0.7h$; $k = 0.4 \times 10^8$ N/m^2, 36 dofs. ○, experimental data; —, stable theoretical solutions; – – –, unstable theoretical solutions.

closely related to the present phenomenon, even if with differences due to the fact that the two interacting modes here do not have the same shape and do not give rise to a traveling wave. A problem of one-to-one-to-two internal resonance has been studied for spherical shallow shells by Thomas et al. [26] with results that have

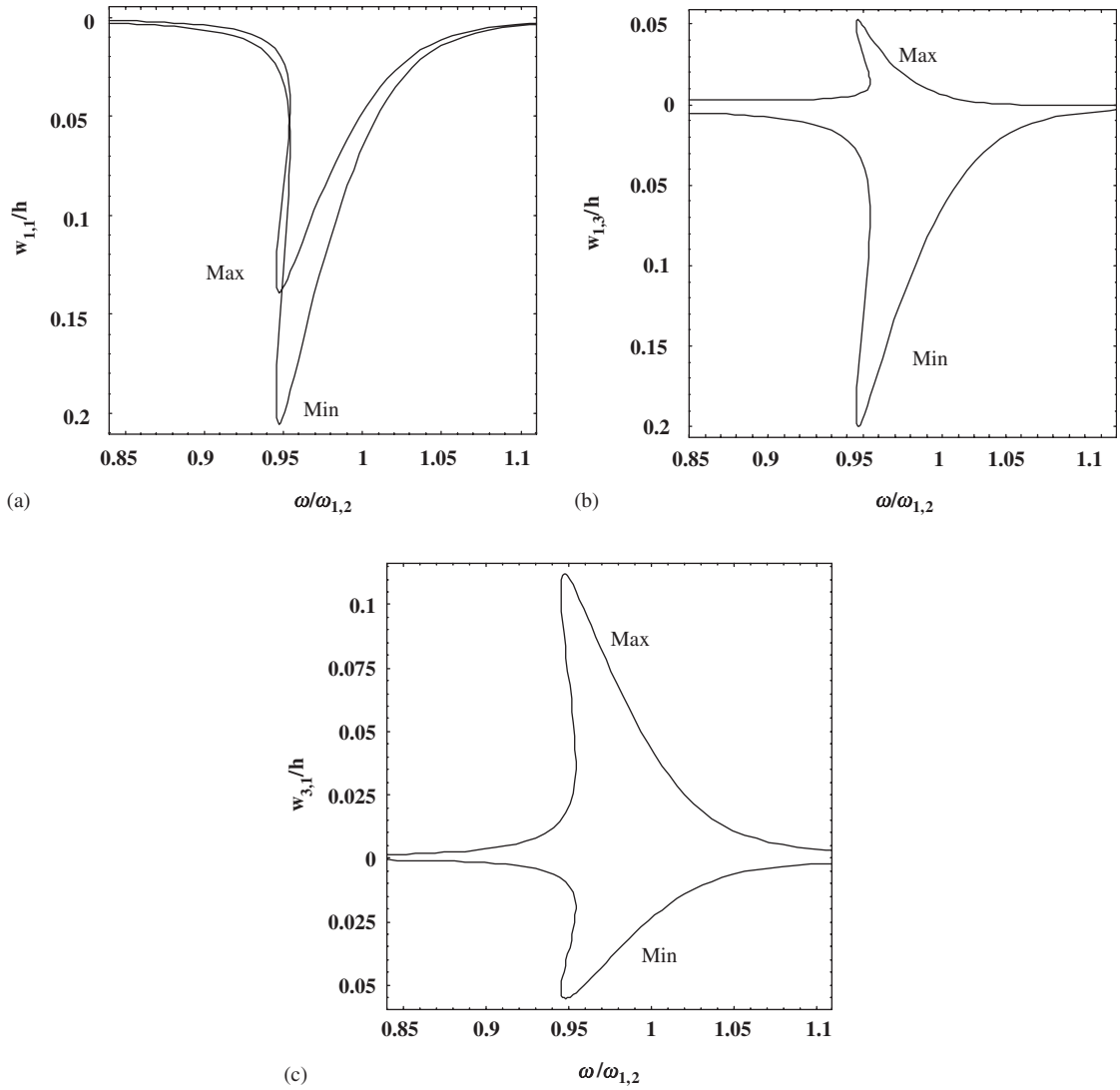

Fig. 28. Response of panel B; mode (1,2), $f = 0.0366$, $\zeta_{1,2} = 0.0162$, $A_{1,1} = 0.7h$; $k = 0$, 36 dofs. (a) Maximum and minimum of the generalized coordinate $w_{1,1}$; (b) maximum and minimum of the generalized coordinate $w_{1,3}$; (c) maximum and minimum of the generalized coordinate $w_{3,1}$.

some relationship with the present ones; different phenomena of internal resonances have been studied by Amabili for circular cylindrical panels [17] and spherical shallow shells [24].

The effect of geometric imperfection $A_{1,1}$ on the nonlinear response of mode (1,2) is investigated in Figs. 26 for the 36 *dofs* models and $k = 0$. Increasing the amplitude of positive imperfection, the nonlinearity (of softening type) is increased.

A comparison of theoretical (36 dofs model with $k = 0.4 \times 10^8\,\mathrm{N/m^2}$) and experimental results for excitation of 0.3 N is shown in Fig. 27 (damping $\zeta_{1,1} = 0.0162$, assumed to be the same for all the generalized coordinates). Comparison of numerical and experimental results is excellent, showing a softening-type nonlinearity. Calculations have been obtained introducing the geometric imperfection $A_{1,1} = 0.7\,\mathrm{h}$, having the form of mode (1,1). With the introduced imperfection and stiffness k, mode (1,2) becomes the fundamental mode, as in the experiments, with natural frequency $\omega_{1,2} = 129.8\,\mathrm{Hz}$ ($\omega_{1,2} = 125.3\,\mathrm{Hz}$ in experiments) and $\omega_{1,1} = 133.5\,\mathrm{Hz}$. In Fig. 27 stability indication is given; only the 1st harmonic of the response is reported because no mean value measurement was effected in this case during experiments.

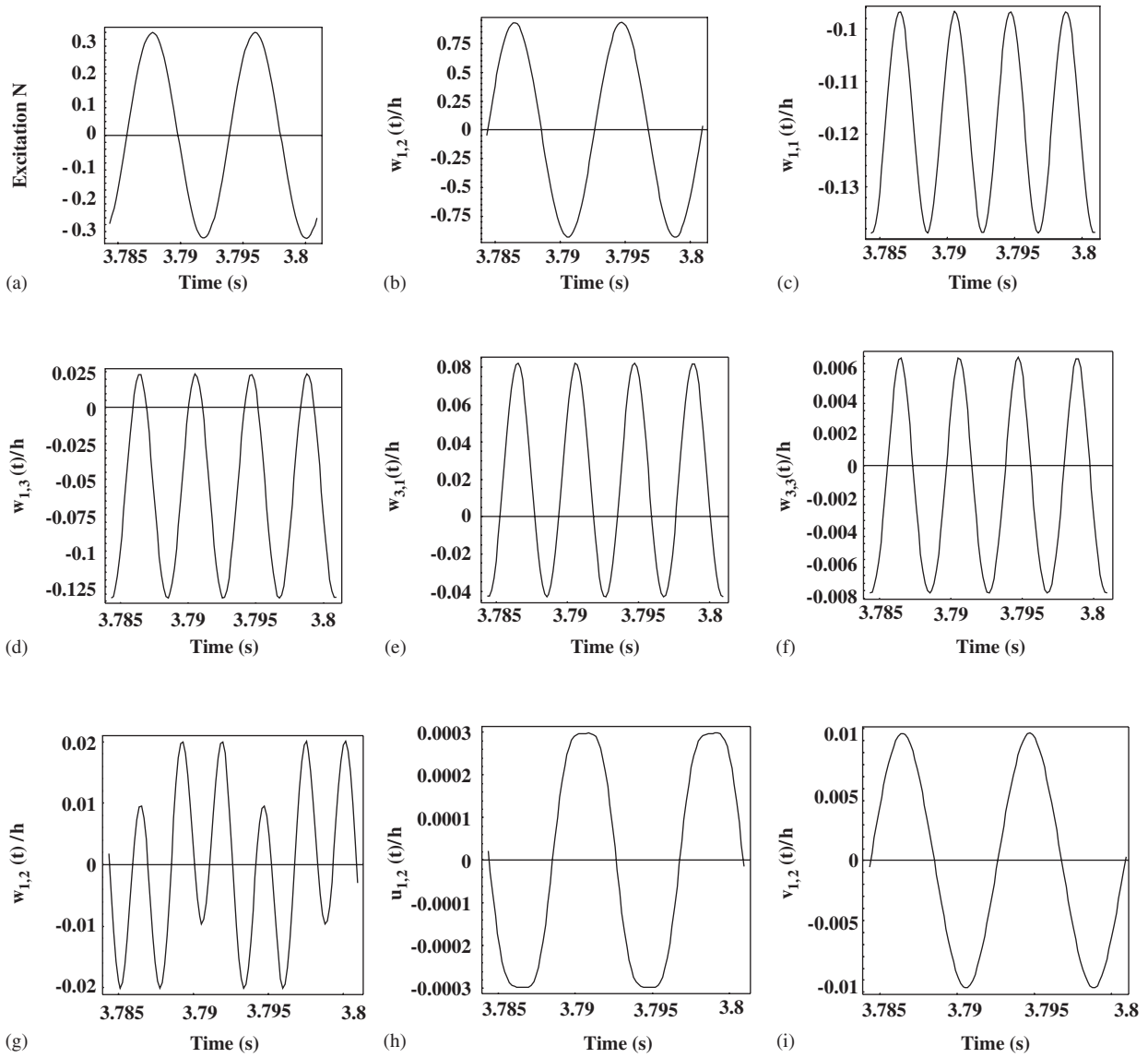

Fig. 29. Computed time response of the panel B for excitation frequency $\omega = 0.97\omega_{1,2}$; fundamental mode (1,2), $f = 0.0366$, $\zeta_{1,2} = 0.0162$, $A_{1,1} = 0.7h$; $k = 0$, 36 dofs. (a) Force excitation; (b) generalized coordinate $w_{1,2}$; (c) generalized coordinate $w_{1,1}$; (d) generalized coordinate $w_{1,3}$; (e) generalized coordinate $w_{3,1}$; (f) generalized coordinate $w_{3,3}$; (g) generalized coordinate $w_{1,4}$; (h) generalized coordinate $u_{1,1}$; and (i) generalized coordinate $v_{0,2}$.

The other three main generalized coordinates ($w_{1,2}$ has been already plotted in Fig. 26) associated to the panel response are reported in Fig. 18 for $k = 0$ and $A_{1,1} = 0.7h$. In particular, the asymmetry of the response of $w_{1,1}$ is reported and shows an always negative (inward) displacement oscillating between a maximum and a minimum plotted in Fig. 28(a). This behaviour is investigated with more accuracy in Fig. 29, where the time response have been plotted for excitation frequency $\omega = 0.97\omega_{1,2}$, i.e. close to the peak of the response; these results have been obtained by direct integration of the equations of motion by using the DIVPAG routine of the Fortran library IMSL, while all the previous ones have been obtained by using AUTO 97. Fig. 29 also indicates the phase relationship with respect to the excitation. The presence of super-harmonics and mean value (zero-frequency) component is clarified in Fig. 30 with the frequency spectra. While $w_{1,2}$ presents only first harmonic component, $w_{1,1}$ presents a very large zero-frequency component and second harmonic, due to quadratic nonlinearity in the equations of motion.

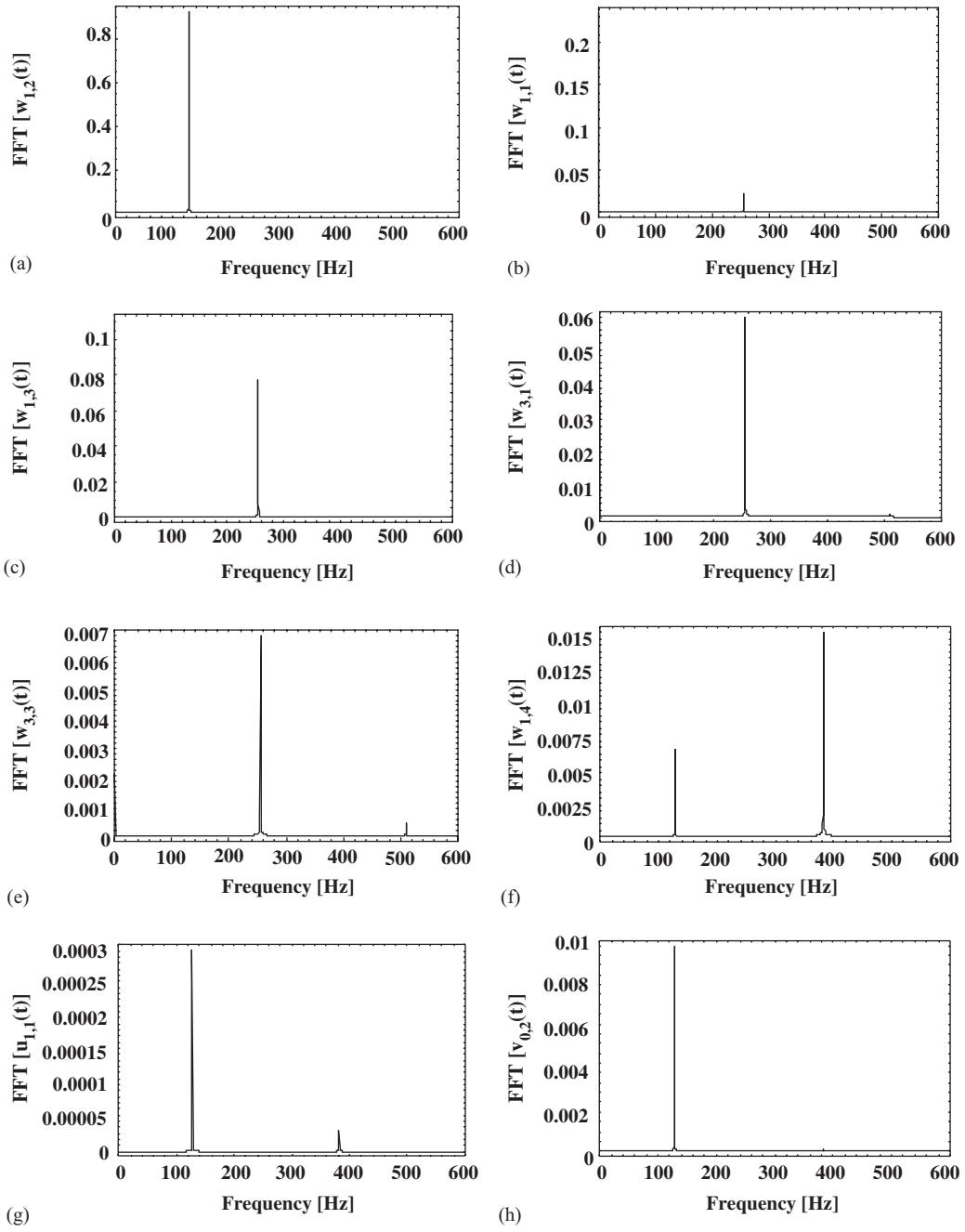

Fig. 30. Frequency spectrum of the response of the panel B for excitation frequency $\omega = 0.97\omega_{1,2}$; fundamental mode (1,1), $f = 0.0366$, $\zeta_{1,2} = 0.0162$, $A_{1,1} = 0.7h$; $k = 0$, 36 dofs. (a) Generalized coordinate $w_{1,2}$; (b) generalized coordinate $w_{1,1}$; (c) generalized coordinate $w_{1,3}$; (d) generalized coordinate $w_{3,1}$; (e) generalized coordinate $w_{3,3}$; (f) generalized coordinate $w_{1,4}$; (g) generalized coordinate $u_{1,1}$; and (h) generalized coordinate $v_{0,2}$.

8. Conclusions

In the present study, for the first time, numerical and experimental results are compared for large-amplitude vibrations of circular cylindrical panels in the frequency range around the fundamental resonance. Comparison is very satisfactorily for both modes (1,1), fundamental mode of panel A, and (1,2), fundamental

mode of panel B. It must be observed that numerical results for higher modes than (1,1) are very scarce in the literature and indicates hardening-type nonlinearity. The present results for mode (1,2) are of extreme interest because (i) they explain for the first time the role of tangential boundary conditions on the nonlinearity of the panel, and (ii) show softening-type nonlinearity for both the numerical model and the laboratory experiments.

The role of geometric imperfections on natural frequencies and nonlinear response is investigated, as well as the role of elastic tangential boundary conditions. Convergence of the solution with the number of generalized coordinates included in the model is discussed. Moreover, the nonlinear phenomenon of one-to-one internal resonance has been detected and investigated numerically for panel B, giving rise to a second branch in the panel response and energy transfer from the mode directly excited to another one.

Acknowledgements

This work was partially supported by the FIRB 2001 and COFIN 2003 grants of the Italian Ministry for University and Research (MIUR). Ing. C. Augenti, Dr. S. Carra, Dr. M. Pellegrini, Ing. S. Sabaini and Ing. M. Venturini are thanked for helping the author in the experiments and some data processing. The support of company BPS (Mario Broggi) at Pero (Milano, Italy), that provided the Polytec laser Doppler vibrometer, is acknowledged.

References

[1] M. Amabili, M.P. Païdoussis, Review of studies on geometrically nonlinear vibrations and dynamics of circular cylindrical shells and panels, with and without fluid-structure interaction, *Applied Mechanics Reviews* 56 (2003) 349–381.
[2] E. Reissner, Nonlinear effects in vibrations of cylindrical shells. Ramo-Wooldridge Corporation Report AM5-6, 1955.
[3] E.I. Grigolyuk, Vibrations of circular cylindrical panels subjected to finite deflections (in Russian), *Prikladnaya Matematika i Mekhanika* 19 (1955) 376–382.
[4] B.E. Cummings, Large-amplitude vibration and response of curved panels, *AIAA Journal* 2 (1964) 709–716.
[5] A.W. Leissa, A.S. Kadi, Curvature effects on shallow shell vibrations, *Journal of Sound and Vibration* 16 (1971) 173–187.
[6] A.S. Vol'mir, A.A. Logvinskaya, V.V. Rogalevich, Nonlinear natural vibrations of rectangular plates and cylindrical panels, *Soviet Physics—Doklady* 17 (1973) 720–721.
[7] D. Hui, Influence of geometric imperfections and in-plane constraints on nonlinear vibrations of simply supported cylindrical panels, *ASME Journal of Applied Mechanics* 51 (1984) 383–390.
[8] L. Librescu, M.-Y. Chang, Effects of geometric imperfections on vibration of compressed shear deformable laminated composite curved panels, *Acta Mechanica* 96 (1993) 203–224.
[9] C.Y. Chia, Nonlinear analysis of doubly curved symmetrically laminated shallow shells with rectangular platform, *Ingenieur-Archiv* 58 (1988) 252–264.
[10] Y.M. Fu, C.Y. Chia, Multi-mode non-linear vibration and postbuckling of anti-symmetric imperfect angle-ply cylindrical thick panels, *International Journal of Non-Linear Mechanics* 24 (1989) 365–381.
[11] R.A. Raouf, A qualitative analysis of the nonlinear dynamic characteristics of curved orthotropic panels, *Composites Engineering* 3 (1993) 1101–1110.
[12] R.A. Raouf, A.N. Palazotto, On the non-linear free vibrations of curved orthotropic panels, *International Journal of Non-Linear Mechanics* 29 (1994) 507–514.
[13] T. Yamaguchi, K. Nagai, Chaotic vibration of a cylindrical shell-panel with an in-plane elastic-support at boundary, *Nonlinear Dynamics* 13 (1997) 259–277.
[14] A.A. Popov, J.M.T. Thompson, J.G.A. Croll, Bifurcation analyses in the parametrically excited vibrations of cylindrical panels, *Nonlinear Dynamics* 17 (1998) 205–225.
[15] K. Nagai, S. Maruyama, M. Oya, T. Yamaguchi, Chaotic oscillations of a shallow cylindrical shell with a concentrated mass under periodic excitation, *Computers and Structures* 82 (2004) 2607–2619.
[16] Y. Kobayashi, A.W. Leissa, Large amplitude free vibration of thick shallow shells supported by shear diaphragms, *International Journal of Non-Linear Mechanics* 30 (1995) 57–66.
[17] M. Amabili, Nonlinear vibrations of circular cylindrical panels, *Journal of Sound and Vibration* 281 (2005) 509–535.
[18] A. Abe, Y. Kobayashi, G. Yamada, Non-linear vibration characteristics of clamped laminated shallow shells, *Journal of Sound and Vibration* 234 (2000) 405–426.
[19] M. Amabili, M. Pellegrini, M. Tommesani, Experiments on large-amplitude vibrations of a circular cylindrical panel, *Journal of Sound and Vibration* 260 (2003) 537–547.
[20] A.W. Leissa, Vibration of Shells, NASA SP-288, Government Printing Office, Washington, DC, 1973, re-issued by The Acoustical Society of America, 1993.

[21] M. Amabili, Comparison of shell theories for large-amplitude vibrations of circular cylindrical shells: Lagrangian approach, *Journal of Sound and Vibration* 264 (2003) 1091–1125.
[22] S. Wolfram, *The Mathematica Book*, fourth ed., Cambridge University Press, Cambridge, UK, 1999.
[23] E.J. Doedel, A.R. Champneys, T.F. Fairgrieve, Y.A. Kuznetsov, B. Sandstede, X. Wang, *AUTO 97: Continuation and Bifurcation Software for Ordinary Differential Equations (with HomCont)*, Concordia University, Montreal, Canada, 1998.
[24] M. Amabili, Non-linear vibrations of doubly curved shallow shells, *International Journal of Non-Linear Mechanics* 40 (2005) 683–710.
[25] M. Amabili, Theory and experiments for large-amplitude vibrations of empty and fluid-filled circular cylindrical shells with imperfections, *Journal of Sound and Vibration* 262 (2003) 921–975.
[26] O. Thomas, C. Touzé, A. Chaigne, Non-linear vibrations of free-edge thin spherical caps: modal interaction rules and 1:1:2 internal resonance, *International Journal of Solids and Structures* 42 (2005) 3339–3373.